


RESEARCH

Open Access



RETSAT associates with DDX39B to promote fork restarting and resistance to gemcitabine based chemotherapy in pancreatic ductal adenocarcinoma

Qiu Tu^{1,2†}, Xiuyun Liu^{1,2,3†}, Xiaoqing Yao^{1,3,4,5†}, Ruixue Li^{6†}, Gaojing Liu^{1,2†}, Honglv Jiang⁷, Kaiqin Li^{1,2}, Qiongfang Chen^{1,2}, Xiaoyan Huang^{1,2,3}, Qing Chang^{1,2,8}, Guoqiang Xu^{7*}, Hong Zhu^{6*}, Peng Shi^{1,4,5*} and Bo Zhao^{1,2,8*} 

Abstract

Background: Severe hypoxia is a prominent character of pancreatic ductal adenocarcinoma (PDAC) microenvironment. In the process of gemcitabine based chemotherapy, PDAC cells are insulted from replication stresses co-induced by hypoxia and gemcitabine. However, PDAC cells get outstanding abilities to resist to such harsh conditions and keep proliferating, causing a major obstacle for current therapy. *RETSAT* (Retinol Saturase) is defined as a hypoxia convergent gene recently, with high expression in PDAC hypoxic sectors. This study aimed to explore the roles of *RETSAT* in replication stress resistance and hypoxia adaptation in PDAC cells, and decipher the underlying mechanism.

Methods: The expression of *RETSAT* was examined in TCGA (The Cancer Genome Atlas), human pancreatic cancer microarray, clinical specimens and cell lines. Functions of *RETSAT* were studied by means of DNA fiber assay and comet assay in monolayer cultured PDAC cell lines, three dimensional spheroids, patient derived organoids and cell derived xenograft mouse models. Mechanism was investigated by using iPOND (isolate proteins on nascent DNA) combined with mass spectrometry, immunoprecipitation and immunoblotting.

[†]Qiu Tu, Xiuyun Liu, Xiaoqing Yao, Ruixue Li and Gaojing Liu contributed equally to this work.

*Correspondence: gux2002@suda.edu.cn; zhuhong@kmmu.edu.cn; ship@mail.kiz.ac.cn; zhaobo@mail.kiz.ac.cn

⁵ Center for Excellence in Animal Evolution and Genetics, Chinese Academy of Sciences, Kunming, China

⁶ Department of Hepatobiliary and Pancreatic Surgery, Second Affiliated Hospital of Kunming Medical University, Kunming, China

⁷ Jiangsu Key Laboratory of Neuropsychiatric Diseases and College of Pharmaceutical Sciences, Jiangsu Key Laboratory of Preventive and Translational Medicine for Geriatric Diseases, Soochow University, Soochow, China

⁸ Primate Facility, National Research Facility for Phenotypic & Genetic Analysis of Model Animals, and National Resource Center for Non-Human Primates, Kunming Institute of Zoology, Chinese Academy of Sciences, Kunming, China

Full list of author information is available at the end of the article



Results: First, we found the converse relationship of *RETSAT* expression and PDAC chemotherapy. That is, PDAC patients with high *RETSAT* expression correlated with poor survival, while ones holding low *RETSAT* expression were benefitted more in Gemcitabine based chemotherapy. Second, we identified *RETSAT* as a novel replication fork associated protein. HIF-1 α signaling promotes *RETSAT* expression under hypoxia. Functionally, *RETSAT* promoted fork restarting under replication stress and maintained genomic stability. Third, we uncovered the interaction of *RETSAT* and R-loop unwinding helicase *DDX39B*. *RETSAT* detained *DDX39B* on forks to resolve R-loops, through which avoided fork damage and *CHK1* initiated apoptosis. Targeting *DDX39B* using chemical CCT018159 sensitized PDAC cells and organoids to gemcitabine induced apoptosis, highlighting the synergetic application of CCT018159 and gemcitabine in PDAC chemotherapy.

Conclusions: This study identified *RETSAT* as a novel replication fork protein, which functions through interacting with *DDX39B* mediated R-loop clearance to promote fork restarting, leading to cellular resistance to replication stresses co-induced by tumor environmental hypoxia and gemcitabine in pancreatic ductal adenocarcinoma.

Keywords: *RETSAT*, *DDX39B*, Fork restarting, Hypoxia, Gemcitabine, Resistance

Background

Severe hypoxia is a common character of pancreatic ductal adenocarcinoma (PDAC). Different from other solid tumors, PDAC consists of dense stromal fibroblasts and inflammatory cells, with abnormal or absent vascularization in central sectors, resulting in over-desmoplasia and quite limited oxygen diffusion through the tumor [1], with median 0.3% oxygen in its tumor microenvironment (TME) [2]. Indeed, TME hypoxia-based therapeutic strategies have been studied and developed over years [3]. The adaptive mechanisms of PDAC cells to hypoxia has been deciphered regarding multiple aspects such as metabolic reprogramming [4, 5], redox homeostasis [6], stemness maintenance [7] and angiogenesis [8]. Many antagonists / agonists of HIF pathway and prodrugs targeting TME hypoxia have been developed [9], and some of them showed ideal therapeutic effects in both xenograft animal models and pre-clinical evaluation [10]. However, the PDAC clinical therapy is still regrettable, with 90% PDAC exhibits resistance to gemcitabine-based therapy, which is the first-line drug for PDAC treatment [11, 12], and 74% relapse post treatment [13, 14]. Thus, it is a major unmet clinical need to understand how PDAC cells are resistant to TME hypoxia.

Sufficient oxygen supply is necessary to DNA synthesis. Ribonucleotide reductase (RNR) is an enzyme consisting of two homodimeric subunits, RRM1 and RRM2 or RRMB2. RNR acts for dNTPs biosynthesis. The β subunit encoded by RRM2 or RRMB2 contains an oxygen-requiring di-iron tyrosyl radical site essential for catalysis [15]. Severe hypoxia challenges the activity of RRM2 β subunit and dNTPs level, which further induces replication stress [16]. One mechanism has been revealed that cells switch RRM1/RRM2 to RRM1/RRM2B enzyme under hypoxia in order to retain activity and preserve ongoing replication, even with much lower fork velocity [17]. Notably, gemcitabine blocks the catalytic domain of RNR to

destroy dNTP pool [11, 12], leading to inhibition of DNA synthesis and cell cycle progression [18].

Apart from these exogenous threats, RNA-DNA hybrid named R-loop is a major obstacle in replication fork progression endogenously [19]. R-loop is formed during mRNA transcription and exists throughout the whole genomes. Especially, there are frequent collisions occurred between replication forks and transcriptional machinery in fast proliferating cells. Indeed, a few cleaners are working over the whole genome to remove R-loop structures in order to orchestrate DNA replication and transcription [20]. For example, RNase H1 is able to digest RNA component of R-loop [21], while *DDX39B* functions as a resolvase to unwind R-loop structures [22]. Persistence replication stress initiates ATR-CHK1 signaling to arrest cell cycle for DNA repair, or launches apoptosis if damage overwhelmed. Alternatively, cells use tolerant mechanisms to adapt to replication stress either through dormant origin firing [23], or through restarting replication downstream of the lesion and leaving behind an ssDNA gap [24]. This means in the process of gemcitabine based chemotherapy, PDAC cells face with replication stresses not only from gemcitabine toxicity and TME hypoxia exogenously, but also from R-loop endogenously. On one hand, PDAC cells must keep DNA synthesis for cell proliferation. On the other hand, they have to protect from fork damage and ATR-CHK1 signaling initiated apoptosis challenged by such harsh conditions [25]. The molecular mechanism underlying this paradox remains to be elucidated.

RETSAT (official name: all trans retinol 13,14 reductase) is an oxidoreductase with conserved protein sequence and genic organization between human and rodent homologs [26]. It plays roles in endoplasmic reticulum (ER) in cytoplasm to transform retinol into 13,14-dihydroretinol. PPAR α in liver [27], PPAR γ in adipose tissue [28] and FOXO1 in primary hepatocytes [29]

function as upstream regulators of RETSAT expression. However, recent studies indicate that its functions might be more than its name suggested [30]. For instance, RETSAT protects fibroblasts from ultra violet (UV) or paraquat induced oxidative stress [31], indicating unknown functions of RETSAT in oxidative homeostasis, or even UV induced DNA damage response and genomic stability. Using evolutionary genome comparison, we identified *RETSAT* to be a convergent gene in mammalian adaptation to hypoxia on the Qinghai-Tibetan Plateau, and the amino acid switch from glutamine (Q) to arginine (R) at the position 247 (Q247R) of RETSAT is responsible for heart function enhancement and mammalian adaptation to hypoxia [32]. *RETSAT* mutation is correlated to occurrence of undifferentiated tongue sarcoma [33], and its expression is positively associated with tumor immune infiltration [34]. Notably, aside from the ER localization, either ectopically expressed or endogenous RETSAT protein has obvious nuclear location [26, 35]. However, the exact nuclear functions of RETSAT are still misty.

In this study, we identified RETSAT as a novel replication fork binding protein. HIF-1 α signaling promotes RETSAT expression under severe hypoxia. RETSAT associates with DDX39B on forks to unwind R-loops and promotes fork restarting, through which protects PDAC cells from fork damage and CHK1 initiated apoptosis. Targeting DDX39B using chemical CCT018159 sensitized PDAC cells and organoids to gemcitabine therapy.

Materials and methods

Cell lines and culture

The human pancreatic cancer cell lines PANC-1 and BxPC-3 were purchased from Conservation Genetics CAS Kunming Cell Bank (Yunnan, China) and validated with short tandem repeat (STR) profiling. The human pancreatic duct epithelial cells HPDE6-C7 were obtained from China Center for Type Culture Collection (Hubei, China). Gemcitabine resistant PANC-1 subline (PANC-1/Gem-R) was purchased from China Center for Type Culture Collection (Hubei, China). PANC-1, BxPC-3 and HPDE6-C7 were cultured in RPMI-1640 containing 10% fetal bovine serum (Gibco, Cat. no.10099141C), 100 U/mL penicillin (Life Technologies, Cat. no. 15140122), and 100 mg/mL streptomycin (Life Technologies, Cat. no. 15140148). PANC-1/Gem-R cells were cultured in RPMI-1640 containing 10% fetal bovine serum (Gibco, Cat. no.10099141C), 100 U/mL penicillin (Life Technologies, Cat. no. 15140122), and 100 mg/mL streptomycin (Life Technologies, Cat. no. 15140148) and 2.5 μ g/ml Gemcitabine (Selleck, Cat. no.s1714). All cells were regularly tested and confirmed for free of mycoplasma contamination using the LookOut Mycoplasma PCR detection (Sigma, Cat. No. MP0035).

Reagents and antibodies

Thymidine was purchased from Sigma (Cat. no. T1895). Bromodeoxyuridine (BrdU) was purchased from Sigma (Cat. no. B5002). 5-ethynyl-2'-deoxyuridine (EdU) was purchased from Life Technologies (Cat. no. A10044). 5-Iodo-2'-deoxyuridine (IdU) was purchased from Sigma (Cat. no. I7125). 5-chloro-2'-deoxyuridine (CIdU) was purchased from Sigma (Cat. no. C6891). Hydroxyurea (HU) was purchased from Sigma (Cat. no. H8627). Gemcitabine was purchased from Selleck (Cat. no. LY-188011). (T2AG3)-Cy3-labeled peptide nucleic acid telomeric probe was purchased from PANAGENE (Cat. no. F2001). Biotin-azide was purchased from Life Technology (Cat. no. B10184). Matrigel was purchased from BD Bioscience (Cat. no. 356234). D-Luciferin was purchased from BioVision (Cat. no. 7903). Green-fluorescent caspase 3/7 probe reagent was purchased from Invitrogen (Cat. no. R37111). SYBRTM Green was purchased from Life Technologies (Cat. no. A25778). FITC Annexin V apoptosis detection kit was purchased from BD Pharmingen (Cat. no. 556547). Low melting agarose was purchased from sigma (Cat. no. A9414). CHK1 antagonist PF47736 was purchased from MedChemExpress (Cat. no. HY-10032). ATR antagonist VE-821 was purchased from MedChemExpress (Cat. no. HY-14731). HIF1 α antagonist PX-478 was purchased from MedChemExpress (Cat. no. HY-10231). HIF2 α antagonist PT-2385 was purchased from MedChemExpress (Cat. no. HY-12867). Glycine was purchased from Sangon Biotech (Cat. no. A100167). Aprotinin was purchased from Sigma (Cat. no. A6103). Leupeptin was purchased from Sigma (Cat. no. L2884). Subcellular Protein Fractionation Kit was purchased from Thermo fisher (Cat. no. L78840). Streptavidin-agarose beads were purchased from Thermo fisher (Cat. no. 11205D). Organoid Dissociation Solution was purchased from BioGenous (Cat. no. E238001).

The following antibodies were obtained from the indicated suppliers: Rabbit anti-RETSAT (Invitrogen, Cat. no. PA5-65443, 1:500 for immunofluorescence and 1:200 for immunohistochemistry and 1:1000 for immunoblotting). Rat anti-BrdU (Abcam, Cat. no. 6326, 1:1000 for immunofluorescence). Rabbit anti-Phospho-Histone H2A.X(Ser139) (Cell Signaling Technology, Cat. no. 9718, 1:1000 for immunoblotting and 1:500 for immunofluorescence). Rabbit anti-DDX39B (Proteintech, Cat. no. 14798-1-AP, 1:500 for immunofluorescence and 1:1000 for immunoblotting). Mouse anti-DNA-RNA Hybrid [S9.6] (Kerafast, Cat. no. ENH001, 1:200 for immunofluorescence and 1:1000 for immunoblotting). Mouse anti-dsDNA (Santa Cruz, Cat. no.sc-58,749, 1:1000 for immunoblotting). Mouse anti-CHK1 (Cell Signaling Technology, Cat. no. 2360, 1:1000 for immunoblotting). Rabbit anti-Phospho-CHK1 (Ser345) (Cell

Signaling Technology, Cat. no. 2348, 1:1000 for immunoblotting). Rabbit anti-Cleaved Caspase-3 (Cell Signaling Technology, Cat. no. 9664, 1:1000 for immunofluorescence). Mouse anti-Ki67 (Vector Laboratories, cat. no. VP-K452). Rabbit anti-ATR (Cell Signaling Technology, Cat. no. 2790, 1:1000 for immunoblotting). Rabbit anti-Phospho-ATR (Ser428) (Cell Signaling Technology, Cat. no. 2853, 1:1000 for immunoblotting). Mouse anti-H2B (Abcam, Cat. no. ab204463, 1:1000 for immunoblotting). Mouse anti-GAPDH (Cell Signaling Technology, Cat. no. 97166, 1:1000 for immunoblotting). Mouse anti-CK19 (Santa Cruz, Cat. no. sc-376,126, 1:200 for immunofluorescence). Rabbit anti-SMARCAL1 (Proteintech, Cat. no. 12513-1-AP, 1:1000 for immunoblotting). Rabbit anti-BLM (Affinit, Cat. no. DF13252, 1:1000 for immunoblotting). The secondary antibodies used for immunofluorescence were raised against rat (conjugated with Cyanine3, ThermoFisher, Cat. no. A-10522), rabbit (conjugated with Alexa 488, ThermoFisher, Cat. no. A-11008; conjugated with Alexa 555, ThermoFisher, Cat. no. A32732) or mouse (conjugated with Alexa 488, ThermoFisher, Cat. no. A11029; conjugated with Alexa 555, ThermoFisher, Cat. no. A31570). The secondary antibodies used for immunoblotting were raised against rabbit (conjugated with HRP, ThermoFisher, Cat. no. 31460) or mouse (conjugated with HRP, ThermoFisher, Cat. no. 31430).

Constructs and lentiviral infection

The guide RNA (gRNA) sequences of *RETSAT* were obtained from GenScript's gRNA Database (www.genscript.com/gRNA-database.html) and cloned into the lentiCRISPR v2 plasmid (Addgene plasmid # 52961) by Esp3I digestion (ThermoFisher, Cat. no. ER0451). The sequence of *RETSAT* gRNA was GGTGCTGGAACAACATACCA. pTomo-Luciferase-IRES-puro was constructed by replacing the RFP in pTomo-empty vector (Addgene plasmid #26291) with Luciferase by XbaI/BamHI digestion, the EGFP was replaced with puromycin resistant gene with BamHI/SalI digestion. pTomo-EF1a-Flag RNase H1 was constructed by inserting EF1 α promoter in pTomo-empty by ClaI/XbaI digestion, and then inserted the 3 \times Flag labeled RNase H1 fragment by XbaI/SalI digestion. The short hairpin RNAs shRNA targeting *DDX39B*, *BLM* and *SMARCAL1* were cloned into the pLKO.1-TRC cloning vector plasmid (Addgene plasmid # 10878) by AgeI/EcoRI digestion. Sequences of *DDX39B* shRNA 1# was: Forward: 5'-CCGGCCTCAACCTCAAACACA TTAACCTCGAGTTAATGTGTTTGAGGTTGAGGTT TTTG-3'; Reverse: 5'-AATTCAAAAACCTCAAACCTCAAACATTAACCTCGAGTTAATGTGTTTGAGGTT GAGG-3'. Sequences of *DDX39B* shRNA 2# was: Forward: 5'- CCGGTGCCGCAAGTTCA TGCAAGATC

TCGAGATCTTGCATGAACTTGCGGCATTTTTG-3'; Reverse: 5'- AATTCAAAAATGCCG CAAGTTCAT GCAAGATCTCGAGATCTTGCATGAACTTGCGGC A-3'. Sequences of *BLM* shRNA 1# was: Forward: 5'- CCGGGACGCTAGACAGATAAGTTTACTCGAGTA AACTTATCTGTCTAGCGTCTTTTTG-3'; Reverse: 5'- AATTCAAAAAGACGCTAGACAGATAAGTTT ACT CGAGTAACTTATCTGTCTAGCGTC-3'. Sequences of *BLM* shRNA 2# was: Forward: 5'- CCGGACCGA ATCTCAATGTACATAGCTCGAGCTA TGTACATTG AGATTCCGTTTTTTG-3'; Reverse: 5'- AATTCAAAA AACCGAATCTCAATGTACATAGCTC GAGCTA TGTACATTGAGATTCCGGT-3'. Sequences of *SMARCAL1* shRNA 1# was: Forward: 5'- CCGGGGAACTCA TTGCAGTGTTTAACTCGAGTTAAACACTGCAAT GAGTTCCTTTTTG-3'; Reverse: 5'- AATTCAAAA AGGAACTCATTGCAGTGTTTAACTCGAGTTAAA CACTGCAATGAGTTCC-3'. Sequences of *SMARCAL1* shRNA 2# was: Forward: 5'- CCGGTGCCCTCATTC TCTTCTTCAACCTCG AGGTTGAAGAAGAGAATG AGGGCATTTTTTG -3'; Reverse: 5'- AATTCAAAA ATGCCCTCATTCTCTT CTTCAACCTCGAGGTTGA AGAAGAGAATGAGGGCA -3'.

The lentiviral vectors were transfected into HEK293T cells along with the packaging plasmids pCMV Δ 8.9 and pMD2.G at a ratio of 5:2.5:1 using Lipofectamine 3000 (Invitrogen, Cat. no. L3000015). Lentivirus was harvested 48 hours post transfection and filtered with 0.45 μ m filter (Millipore, Cat. no. SLHV033RB). Pancreatic cancer cells were infected with lentiviruses and screened with 3 μ g/mL puromycin 72 hours post infection.

Immunofluorescence

Immunofluorescence was performed as described previously [36]. Specifically, for co-localization analysis of *RETSAT* with BrdU-labeled replication foci, cells were pulse labeled with 10 μ M BrdU for 5 minutes. After 4% Paraformaldehyde fixation and treatment with 2N HCl (Hydrochloric acid) at 4°C overnight, cells were washed with PBS for three times to remove residual HCl, treated with 0.3% Triton X-100 for 15 minutes, and blocked by 10% goat serum for 1 hour at room temperature. Then cells were incubated overnight at 4°C with primary antibodies, and then labeled by fluorescent second antibodies for 1 hour at room temperature. Nucleus was stained by DAPI. Images were captured using confocal microscope system (Olympus, FV1000).

Immunoblotting

Cells were lysed in RIPA buffer containing protease inhibitor cocktail (ThermoFisher, Cat. no. 87786) and centrifuged to remove the debris. Concentration of supernatant protein was quantified with BCA method

(Beyotime; Cat. no. P0009). Standard SDS-PAGE gel electrophoresis was performed, followed by blocking with 5% skimmed milk and immunoblotting with primary antibodies at 4°C overnight. Specific signals were detected with horseradish peroxidase-conjugated secondary antibodies and chemiluminescent horseradish peroxidase substrate reagents (Millipore, Cat. no. WbKLS0500). Images were captured using automatic chemiluminescence imaging analysis system (Tanon, 5200).

Dot blotting

Cells were trypsinized and washed twice with ice-cold PBS, and lysed by cell lysis buffer (0.5% NP-40, 80 mM KCl, 5 mM PIPES) for 10 minutes. The nuclear was obtained through centrifuge at 500 x g for 5 minutes, and lysed with nuclear lysis buffer (1% SDS, 25 mM Tris-HCl pH8.0, 5 mM EDTA) for 10 minutes. Lysis was added into 3 µL 20 mg/mL proteinase K and incubate for 3–5 hours at 55°C. Extraction was performed twice using phenol:chloroform:isoamyl alcohol (25:24:1, pH8.0) and chloroform, followed by 3 M sodium acetate (pH5.2), glycogen and ice-cold 100% ethanol. After spinning down at 12,000 x g for 30 minutes at 4°C and washing with 1 mL 70% ethanol, the pellet was resuspended into elution buffer (10 mM Tris-Cl, pH8.5). Genomic DNA was diluted in 50 µL TE buffer and spotted onto Hybond N+ membrane (GE Healthcare) using a Bio-Dot Apparatus (Bio-Rad, Cat. no.1706545). The membrane was blocked with 5% skim milk at room temperature after ultraviolet (UV) (0.24J) cross-linking for 1 hour. The membrane was incubated with S9.6 antibody or dsDNA antibody overnight at 4°C, followed by procedures as same as immunoblotting described above.

Immunohistochemistry

PDAC microarray was purchased from Shanghai Outdo Biotech (HPan-Ade180Sur-01). The clinical pancreatic tumor tissues were obtained from The Second Affiliated Hospital of Kunming Medical University. The protocol was approved by the Human Resource Use Committee of The Second Affiliated Hospital of Kunming Medical University. The immunohistochemistry (IHC) was performed as described [37]. Briefly, sections were deparaffinized and rehydrated, and antigen retrieval was performed in citric acid solution (pH6.0) for 5 minutes at 125°C in an autoclave. Endogenous peroxidase activity was quenched by incubation in 3% hydrogen peroxide for 15 minutes, followed by blocking in 10% goat serum for 1 hour at room temperature, incubation overnight at 4°C with primary antibodies, and HRP-DAB staining (Beyotime, cat. no. P0202) or fluorescent secondary antibody. The slides were mounted with Aqua-Poly/Mount (cat. no. 18606; Polysciences, Warminster, PA, USA). Images were

captured using Three-dimensional ultra-depth-of-field microscope VHX-6000 and Olympus optical microscope BX43.

Clone formation assay

Colony formation assay in soft agar was performed as described previously [38]. Basal agarose layer (0.8%) was prepared of 1 mL for one 6-well plate by diluting stock agar solution with growth medium and cooled at 4°C for ~5 minutes. The upper agarose layer (0.48%) was mixed well with 10⁴ cells and immediately dropped onto solidified basal layer, then cooled at 4°C for 5 minutes. One milliliter of growth medium was added. Cells were incubated at 37°C and 5% CO₂ for 20 days. Cultural medium was refreshed every 4–7 days. The clones were staining by 0.005% crystal violet and counted using the dissecting microscope.

Cell apoptosis assay

For monolayer cultured cells, apoptosis analysis was performed by flow cytometry using FITC Annexin V apoptosis detection kit I (BD Pharmingen, Cat. no. 556547) according to manufacturer's guidance. For 3D spheroids, apoptosis analysis was performed by green-fluorescent caspase 3/7 probe reagent and flow cytometry using FITC Annexin V apoptosis detection kit I (BD Pharmingen, Cat. no. 556547) after dissociated with Organoid Dissociation Solution (E238001), green-fluorescent caspase 3/7 probe reagent was added into medium and incubated for 30–60 minutes. The green fluorescence was observed with fluorescence microscope, the density of fluorescence was quantified with Image J software.

Real-time RT-PCR

Total RNA was extracted using Trizol reagent (sigma, Cat. no.T9424). Reverse transcription was carried out using the RevertAid First Strand cDNA Synthesis kit (Thermo Fisher Scientific, Cat.no.K1621). Quantitative real-time PCR was performed using SYBR Select Master Mix kit (Life Technologies, Cat. no. A25778). The primers used for *RETSAT* were: forward 5'-ATTGCCTTC CACACCATC-3', reverse 5'-TTGAACAGTCCTGCG TTG-3'.

Neutral comet assay

The neutral comet assay was performed as described [39]. Briefly, 2 × 10³ cells in 10 µL PBS were added into 70 µL 1% low-melting agarose at 37°C, pipetted and evenly spread onto slide pre-coated with 0.8% agarose. The slides were incubated at 4°C in the dark for 10 minutes, and then transferred into prechilled lysis solution (2.5 M NaCl, 100 mM EDTA, 10 mM Tris-base, 1% sodium lauryl sarcosinate, 1% Triton X-100, pH9.5) for

60 minutes at 4°C. The slides were then transferred to prechilled neutral electrophoresis solution (300 mM sodium acetate, 100 mM Tris, pH=8.3) and subjected to electrophoresis at 15 V/cm, 80 mA for 30 minutes, followed by washing with distilled water and immersed in ice cold 100% ethanol at room temperature for 5 minutes and air dried. DNA was stained with DAPI for 5 minutes. Comets were analyzed using Comet Assay Software Project (CASP) (Andor Technology). A total of 150 cells from different random areas were counted per slide. Each experiment was repeated at least twice independently.

DNA fiber assay

DNA fiber assay was performed as described [40]. Specifically, replicating DNA was first labeled with 25 μM 5-iodo-2'-deoxyuridine for 20 minutes with or without HU treatment. Cells were then subjected to the second labeling with 250 μM 5-chloro-2'-deoxyuridine. After labeling, 2.5 μL of the cell suspension (~2500 cells) were spotted onto one end of the glass slide, followed by addition of 7.5 μL of lysis buffer (50 mM EDTA, 0.5% SDS, 200 mM Tris-HCl, pH7.5). After incubation for 8 minutes at room temperature, the slides were tilted to 15° to allow the DNA fibers to spread down along the slide. DNA fibers were treated with 2.5 M hydrochloric acid and incubated with rat anti-BrdU monoclonal antibody that recognizes CIdU, but not IdU at 4°C overnight, followed by an AlexaFluor cy3-conjugated goat anti-rat secondary antibody for 1 hour at room temperature. The mouse anti-IdU monoclonal antibody that recognizes IdU but not CIdU (4°C overnight) and AlexaFluor 488-conjugated goat anti-mouse secondary antibody (1 hour at room temperature) were used to detect IdU. DNA fibers were analyzed on a Leica DM6000B microscope equipped with a CoolSNAP HQ CCD camera (Roper Scientifics). The lengths of CIdU (AF cy3, red) and IdU (AF 488, green) labeled patches were measured using the Image J software, and μm values were converted into kb using the formula 1 μm=2.59 kb. Two hundred fibers from different random areas were analyzed for assessment of fork dynamics.

Isolate proteins on nascent DNA (iPOND)

iPOND was performed as described [41, 42]. Briefly, pancreatic cancer cells were cultured under normal conditions with or without gemcitabine. Cells were synchronized in S phase by twice treatment of thymidine. For the first time of treatment, cells were treated with 2 mM thymidine for 18 hours, followed by release into thymidine-free medium for 10 hours. Then the second treatment was performed with 2 mM thymidine for 18 hours, and released for 6 hours. Cells were incubated with 10 mM EdU for 10 minutes. After EdU labeling, cells were treated

with or without gemcitabine for 4 hours. Cells were then fixed in 1% formaldehyde, followed by quenching with 0.125 M glycine (Sangon Biotech, A100167). Cells were then collected and washed three times in ice-cold PBS, and permeabilized in ice-cold 0.25% Triton X-100/PBS for 30 minutes. Before click reaction, samples were washed once in 0.5% BSA/PBS and once in ice-cold PBS.

For click reaction, cells were incubated in click reaction buffer for 1 hour at room temperature containing 10 μM Biotin-azide. The “no-click” sample (negative control) used DMSO instead of Biotin-azide. Following the Click reaction, cells were washed once in 0.5% BSA/PBS and once in ice-cold PBS, and resuspended in lysis buffer (50 mM Tris-HCl, pH8.0, 1% SDS) containing 1 μg/mL aprotinin (Sigma, A6103) and 1 μg/mL leupeptin (Sigma, L2884) and sonicated using a Bioruptor™ UCD-200 for 60 cycles (30s pulse/ 30s pause). Samples were centrifuged at 16100×g at 4°C for 10 minutes and the supernatant was collected. The supernatant was filtered through a 90-μm nylon mesh and diluted 1:1 (V/V) with ice cold PBS containing 1 μg/mL aprotinin and 1 μg/mL leupeptin. The input samples were collected. Streptavidin-agarose beads (Thermo fisher, 11205D) were washed three times in lysis buffer containing aprotinin and leupeptin. Two hundred microliter bead slurry was used for 1 × 10⁸ cells. The streptavidin-agarose beads were added to the samples, which were then incubated at 4°C for 16 hours in dark. Following binding, the beads were washed with ice-cold lysis buffer, followed by one wash with 1 M NaCl and two washes with ice-cold lysis buffer. To elute proteins bound to nascent DNA, the 2× SDS Laemmli sample buffer (2× SB) mix (0.4 g SDS, 2 mL 100% Glycerol, 1.25 mL 1 M Tris, pH6.8 and 0.01 g Bromophenol blue in 8 mL H₂O) was added to packed beads (1:1; V/V). Samples were incubated at 95°C for 25 minutes, followed by immunoblotting or mass spectrometry detection.

Mass spectrometry assay

The purified proteins were separated by SDS-PAGE and visualized by silver staining. The gel was then cut into small pieces. Disulfide bonds were reduced, thiols were alkylated, and proteins were digested according to the in-gel trypsin digestion protocol [43]. The extracted peptides were dried, resuspended in 0.1% trifluoroacetic acid, desalted with C18 ZipTips, dried again, and dissolved in 0.1% formic acid.

An Orbitrap Elite hybrid mass spectrometer (MS) with an electrospray ionization inlet (Thermo Fisher) was used to analyze the peptide samples using a previously described method [44]. Briefly, samples were separated on a C18 analytical column through a nanoscale HPLC with solution A of 0.1% formic acid and solvent B of 80% acetonitrile and 0.1% formic acid. The HPLC gradient

was 6 to 44% solvent B for 90 minutes. The automatic data acquisition in positive ion mode in MS was used to collect the 15 strongest ions in each precursor MS scan. Each precursor ion was analyzed twice in 60 seconds. The resolution for the precursor ion was set to 120,000 at 200 m/z and the isolation window of the selected precursor ion for MS/MS analysis was set to 2 m/z.

The MS/MS raw files were searched with Proteome Discoverer (version 2.1, Thermo Fisher Scientific) against the Human UniProt database (www.uniprot.org) with concatenated reverse protein sequence and common contaminants. The parameters used to identify tryptic peptides for the protein identification were a 10 ppm precursor-ion mass tolerance, 0.6 Da production mass tolerance. Enzyme specificity was set to trypsin and a maximum of 2 missed cleavages per peptide were allowed. The cysteine carbamidomethylation was set as fixed modification and methionine oxidation and N-terminal acetylation as variable modifications. The 1% FDR at both peptide and protein levels was applied for the analysis. Relative protein quantification was based on the label-free quantification included in the Proteome Discoverer software package. The Abundance of the protein was obtained from each sample.

Co-immunoprecipitation

Co-immunoprecipitation (Co-IP) was performed as described previously [36]. Specifically, PANC-1 cells were harvested and washed twice with ice-cold PBS and lysed with 1× RIPA lysis buffer (Beyotime, P0013D) containing complete EDTA-free (Roche) inhibitors. Immunoprecipitation with RETSAT antibody performed on and with Lysates were digested by 10 units/mL DNase I (New England Biolabs, M0303), and incubated with anti-RETSAT primary antibody overnight. Isotype IgG were used as negative controls. Immunoprecipitation was carried out using protein A/G Agarose Resin (Yeasen, 36403ES08) according to the manufacturers' protocol. After pulling down and wash, proteins were fractionated by SDS-PAGE gel for immunoblotting.

3D spheroid culture

3D culture of pancreatic cancer cells was performed as previous described [45]. Briefly, Matrigel was diluted with serum-free culture medium to a final concentration of 7 mg/mL. One hundred microliter diluted Matrigel was added into each well of 96-well plate and incubated for 60 minutes in 37°C for solidification. Pancreatic cancer cells were seeded onto Matrigel at a density of 5000 cells/well. Gemcitabine was added the next day post cell seeding and maintained for a total of 7 days, with a mid-week change of fresh medium.

PDAC organoids culture

Primary human PDAC organoids were established from two PDAC surgical biopsies in The Second Affiliated Hospital of Kunming Medical University as previously described [46–48]. Briefly, human PDAC tissues were rinsed with DPBS twice and minced into small fragments of 1–3 mm³, followed by digestion with 10 mL of tumor tissue digestion solution (BioGenous, K601003) in a 15 mL conical tube at 37°C for variable incubation times ranging from 30 min to 90 min. Cells were filtered using a 100 µm cell strainer and centrifuged at 250×g for 3 min at 4°C. Cells were resuspended with AddMEM/F12 (Invitrogen, 12,634–010) and Growth Factor reduced (GFR) Matrigel (Corning, 356,231). Thirty microliter matrigel containing approximately 10,000 cells was loaded onto the bottom of 24-well plates and incubated at 37°C and 5% (*vol/vol*) CO₂ for 25 min for solidification. The culture medium was composed of AddMEM/F12 (basal medium), 1 M HEPES, 1x GlutaMax (Invitrogen, 35,050–061), 1% penicillin/streptomycin (Invitrogen, 15,140,122), 1x B27 (Invitrogen, 17,504,044), 1 mM N-acetyl-L-cysteine (Sigma-Aldrich, 9165), 100 ng/mL Wnt-3a (R&D Systems, 5036-WN-010), 100 ng/mL R-Spondin 1 (Peprotech, 120–38), 100 ng/mL Noggin (Invitrogen, 120-10C), 50 ng/ml epidermal growth factor (Peprotech, AF-100-15), 100 ng/mL fibroblast growth factor (Peprotech, C100–26), 10 mM Nicotinamide (Sigma, N0636), 10 µM Y-27263 (Sigma, Y0503) and 0.5 µM A83–01 (R&D Systems, 2939/10).

Cell Derived Xenograft (CDX) model

Animal care and experimental protocols were approved by the Institutional Animal Care and Use Committee of Kunming Institute of Zoology, Chinese Academy of Sciences. Five to six-week-old B-NDG (NOD-Prkdcscid IL2rgtm1/Bcgen) mice were purchased from Jiangsu Biocytogen Co., Ltd. (Nantong, China) and kept under specific pathogen-free environment. PANC-1 cells were infected with lentivirus expressing Luciferase and selected with 3 µg/mL puromycin for 7 days. 1 × 10⁶ cancer cells in 100 µL PBS containing 30% Matrigel were injected into each B-NDG mouse subcutaneously. To monitor tumor growth by bioluminescent imaging in vivo weekly, the mice were intraperitoneally injected with 150 mg/kg D-Luciferin and imaged using IVIS system followed by analyzed with Living Image software (Caliper Life Science, IVIS Lumina Xr, USA). Mice were treated with 100 µL of vehicle (saline) or gemcitabine at dose of 50 mg/kg by intraperitoneal injection weekly. The mice were sacrificed before tumor volume reached to approximately 2000 mm³.

Statistical analysis

Statistical analysis was performed using GraphPad Prism 9 software (GraphPad Inc., San Diego, CA, USA). Quantitative data are represented as mean \pm s.e.m. unless otherwise stated. Comparisons between two groups were analyzed by two tailed Student's *t*-test for statistical significance. One-way analysis of variances was applied for multiple comparisons. Experiments were repeated three times unless otherwise stated. No samples or animals were excluded from any analyses and all replicates were authentic biological replicates. Animals were randomly assigned to treatment of gemcitabine. Blind analysis was not performed in this study. $P < 0.05$ was considered as significant.

Results

High expression of RETSAT correlated to poor survival in PDAC patients

To study the roles of *RETSAT* in pancreatic cancers, we first downloaded the bulk transcriptional database from TCGA (The Cancer Genome Atlas). Compared with normal pancreatic tissues ($n = 252$ cases), the *RETSAT* mRNA levels were dramatically high in tumor tissues ($n = 174$ cases) ($P = 7.52 \times 10^{-15}$, Fig. 1A). We further examined its expression in non-transformed human pancreatic duct epithelial (HPDE) cell line H6c7 and transformed PDAC cell lines BxPC-3 and PANC-1. Compared to H6c7, *RETSAT* was overexpressed in BxPC-3 and PANC-1 at both mRNA transcription and protein levels (Fig. 1B-C). Notably, PANC-1 cells have *KRAS*^{G12D} and *TP53*^{R273H} mutation genetically. BxPC-3 cells have wide type *KRAS* and *TP53*^{Y220C} mutation [49]. Furthermore, we compared the transcription of *RETSAT* in *KRAS* mutant PDAC tumors ($n = 86$) with *KRAS* wide type counterparts ($n = 10$) in TCGA dataset (Supplementary

Fig. 1A), showing that there was no significant difference ($P = 0.68$). These results indicate that *RETSAT* is highly expressed in transformed PDAC cells regardless of *KRAS* genetic status.

We next focused on 174 PDAC cases used in Fig. 1A. These cases were ranked based on the FPKM (Fragments Per Kilobase Million) of *RETSAT*, and defined as *RETSAT* high (50% of total, 87 cases) or *RETSAT* low (50% of total, 87 cases) subgroups. We found that the *RETSAT* level conversely related to PDAC overall survival, with high *RETSAT* corresponding to poor survival compared with low subgroup ($P = 0.027$, Fig. 1D). For validation, we performed immunohistochemistry (IHC) of *RETSAT* in commercial PDAC microarray, which included 90 PDAC specimens. Compared with own adjacent, the integrated density of *RETSAT* was drastically higher in tumor regions ($P = 0.0026$, Fig. 1E). Based on the ratio of *RETSAT* integrated density in tumor area versus own adjacent. Forty-eight samples with ratios less than 1.5 were defined as low, while 42 samples with ratios greater than 1.5 were defined as high (Fig. 1F). Consistent to analysis from TCGA database, *RETSAT*-high subgroup in PDAC microarray showed significantly poor survival compared with low subgroup ($P = 0.0001$, Fig. 1G). We also collected 80 clinical PDAC specimens for confirmation. As such, the expression of *RETSAT* in 40 cases was quite higher than the rest ones ($P < 0.0001$, Fig. 1H). Through separating them into low (40 cases) and high (40 cases) subgroups (Fig. 1I), we got the similar tendency between *RETSAT* expression and survival ($P = 0.0001$, Fig. 1J).

Among these clinical specimens, 38 cases came from PDAC patients who accepted for PDAC clinical surgery, followed by gemcitabine based chemotherapy. These specimens were originally from clinical operation without any chemical treatments ahead of surgeries. After surgeries, all 38 patients accepted for gemcitabine,

(See figure on next page.)

Fig. 1 High expression of *RETSAT* correlated to poor survival in PDAC patients. **A** The expression of *RETSAT* in PDAC tumor tissues ($n = 174$) from The Cancer Genome Atlas database compare to normal tissues from The Cancer Genome Atlas database and GTEx database ($n = 252$). **B, C** qPCR (**B**) and immunoblotting analysis (**C**) of *RETSAT* in human pancreatic duct epithelial (HPDE) cell line HPDE6-C7, pancreatic cancer cell lines PANC-1 and BxPC-3, the exposure time was 0.2 s (short exposure) and 1 s (long exposure) respectively in (**C**). **D** Kaplan–Meier curve for overall survival of PDAC patients ($n = 174$) with low vs high expression of *RETSAT*. The data was downloaded from TCGA dataset and re-analyzed. **E** Quantification of IHC integrated density of *RETSAT* in PDAC tissue microarray using image J software. Ninety adjacent tissues and corresponding tumor tissues were calculated. **F** Classification of PDAC microarray tissues into *RETSAT* high ($n = 42$) and low ($n = 48$) subgroups based on the ratio of *RETSAT* integrated density in tumor tissues versus own adjacent tissues. Tissues with ratio greater than 1.5 were defined as *RETSAT*-high, while lower than 1.5 were defined as *RETSAT*-low. **G** Overall survival time (months) of *RETSAT*-high and *RETSAT*-low subgroups based on microarray information. The figure shows the Kaplan–Meier survival curves. **H, I** Quantification of IHC integrated density of *RETSAT* in PDAC clinical tissues using image J software (**H**), 80 tumor tissues were calculated and divided into *RETSAT* high ($n = 40$) or low ($n = 40$) subgroups (**I**) based on IHC integrated density of *RETSAT*. **J** Kaplan–Meier curve for overall survival of *RETSAT*-high and *RETSAT*-low subgroups based on clinical information. **K** Representative images of immunohistochemistry staining of *RETSAT* in clinical PDAC tissues. **L** 38 PDAC tissues collected from clinical surgeries ahead of gemcitabine based treatment were classified into *RETSAT* high ($n = 19$) or low ($n = 19$) subgroups based on IHC integrated density of *RETSAT*. **M** Kaplan–Meier curve for overall survival of PDAC patients after surgery and followed by gemcitabine based therapy. Scale bar = 200 μ m in (**K**), $n = 3$ independent experiments unless otherwise stated. All data are presented as mean \pm SEM. *P* values were calculated using a two-tailed student's *t* test

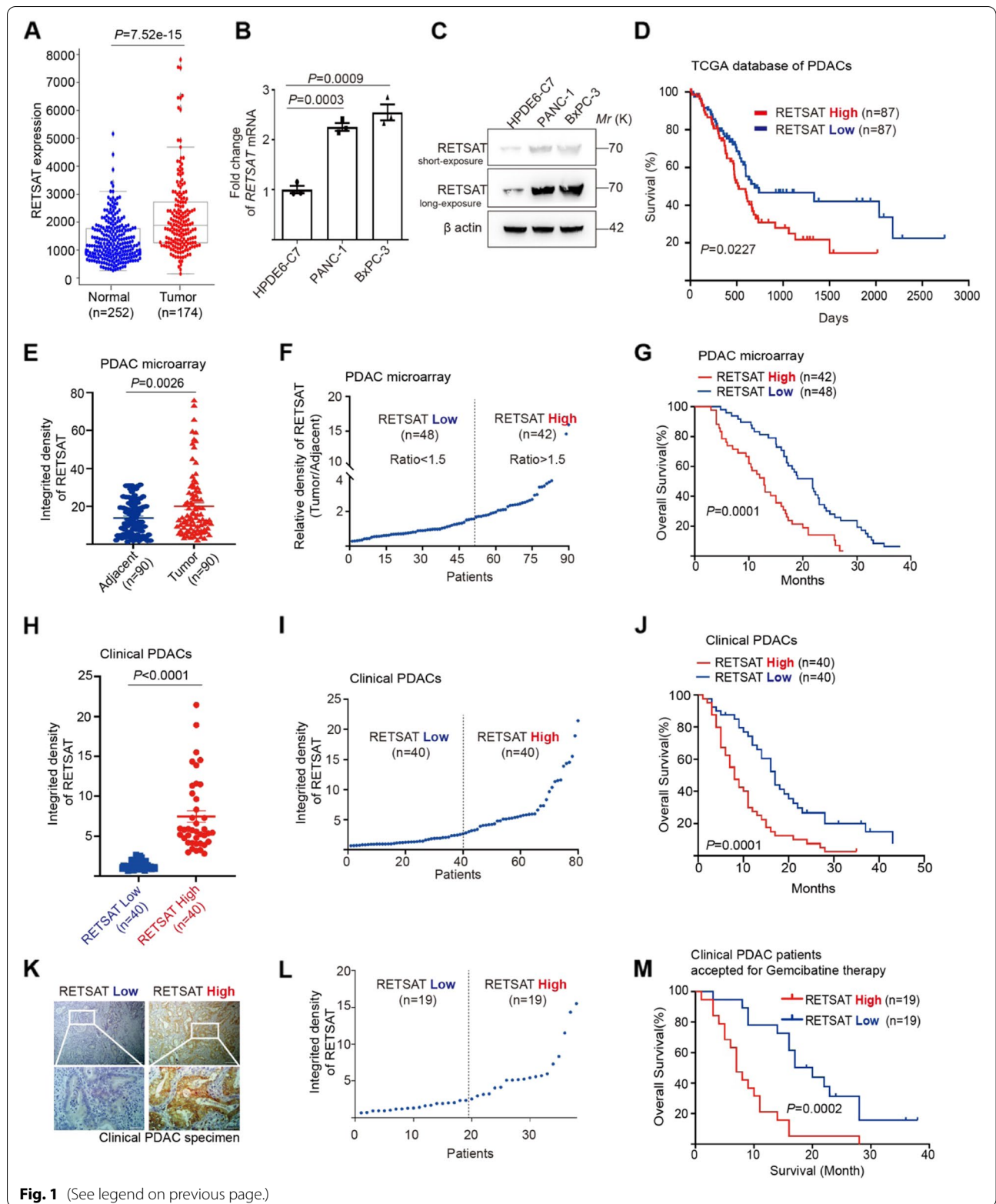


Fig. 1 (See legend on previous page.)

gemcitabine plus Albumin Paclitaxel, gemcitabine plus Cisplatin based therapy. We examined the expression of RETSAT in each specimen by means of IHC. Meanwhile, the survival time of each patient after surgery was confirmed through telephone communication with patients in person or their immediate families. The specimens were ranked based on RETSAT level (Fig. 1K-L). After integrated analysis, we found that patients with low level of RETSAT were benefitted more from gemcitabine therapy ($P=0.0002$, Fig. 1M). Together, these findings support the notion that high RETSAT is related to poor survival in the context of PDAC.

RETSAT deletion sensitized PDAC cells to gemcitabine induced apoptosis

We examined the location of RETSAT in PDAC specimens. Notably, dramatic RETSAT was observed in PDAC ductal regions (Fig. 2A), where has been defined as a major hypoxic area of PDAC [50]. To confirm this, we co-stained RETSAT with hypoxia marker HIF-1 α in PDAC specimens. As shown in Fig. 2B, HIF-1 α positive sectors had quite high level of RETSAT (right zoomed region, Fig. 2B), while HIF-1 α negative sectors showed almost no RETSAT expression (lower zoomed region, Fig. 2B). This reminded us to investigate whether RETSAT is under control of HIF-1 α signaling. To this goal, we cultured PANC-1 and BxPC-3 cells in 0.3% oxygen tension in order to mimic PDAC pathological hypoxia [2]. Cells were collected at consecutive time points for immunoblotting and qRT-PCR. We found that severe hypoxia could increase RETSAT level dramatically (Fig. 2C-E). PX-478 is a selective inhibitor of HIF-1 α [51]. We treated PANC-1 cells with vehicle or 10 μ M PX-478 for 24 hours in 0.3% oxygen tension. Both qRT-PCR and immunoblotting results revealed that PX-478 significantly inhibited RETSAT level (Fig. 2E-G). This indicates that the

upstream HIF-1 α signaling promotes RETSAT expression in PDAC cells under severe hypoxia.

To investigate the roles of RETSAT in PDAC cell fate determination, we derived RETSAT knockout (*RETSAT-KO*) PANC-1 cells from luciferase positive parental (Fig. 2H). Monolayer (2-D) or spheroid (3-D) cultured cells were treated with or without 10 μ M gemcitabine under 21% or 0.3% O₂ oxygen tension for 72 hours, and collected for flow cytometry analysis. Compared to parental counterpart, *RETSAT-KO* cells proliferated more slowly under gemcitabine treatment, as evaluated by anti-Ki67 antibody immunostaining combined with flow cytometry analysis ($P<0.0001$ *RETSAT-KO* versus parental under Gem in Supplementary Fig. 1B-C). Moreover, *RETSAT-KO* cells were more sensitive to apoptosis under gemcitabine and severe hypoxia conditions ($P=0.0004$ *RETSAT-KO* versus parental under Gem and 0.3% O₂ in Fig. 2I-J, $P=0.0014$ *RETSAT-KO* versus parental under Gem and 0.3% O₂ in Supplementary Fig. 1D-G). We validated this result in cell-derived xenografts (CDX) mice model (Fig. 2K). PANC-1 parental and *RETSAT-KO* cells were injected into NOD-SCID immunodeficient mice to form xenografts in parallel. One week post cell injection, mice bearing xenografts were separated into groups randomly for gemcitabine treatment. *RETSAT* knockout has no influence on CDX formation ($P=0.1781$ parental + vehicle versus *RETSAT-KO* + vehicle, Supplementary Fig. 1H-I). After 3 weeks treatment of gemcitabine (50 mg/kg, once per week), gemcitabine suppressed the growth of *RETSAT-KO* tumors with decreased luciferase strength ($P=0.0023$ parental + Gem versus *RETSAT-KO* + Gem, Supplementary Fig. 1J-M), lower tumor size and weight ($P=0.0017$ parental + Gem versus *RETSAT-KO* + Gem, Fig. 2L-N), and prolonged survival time ($P=0.0045$ *RETSAT-KO* versus parental after gemcitabine treatment, Fig. 2O).

(See figure on next page.)

Fig. 2 RETSAT deletion sensitized PDAC cells to gemcitabine induced apoptosis. **A** Representative images of fluorescent Co-immunohistochemistry staining of RETSAT (red) and ductal cell marker CK19 (green) in PDAC tissue microarray. **B** Co-immunohistofluorescence of RETSAT (red) and HIF-1 α (green) in PDAC tissue. **C, D** Immunoblotting (**C**) and quantification (**D**) of RETSAT in PDAC cell lines PANC-1 and BxPC-3. Cells were cultured under normoxia (21% O₂) or hypoxia (0.3% O₂) for 12, 24, 48, 72 hours respectively. β actin was used as a loading control. **E** qPCR analysis of *RETSAT* transcription under indicated treatments. HIF-1 α antagonist PX-478 (10 μ M) was used. **F, G** Immunoblotting (**F**) and quantification (**G**) of RETSAT in PANC-1 cells under indicated treatments. **H** Immunoblotting confirmation of RETSAT deletion in luciferase positive PANC-1 cells. **I, J** Representative images (**I**) and quantification (**J**) of apoptosis using green-fluorescent caspase 3/7 probe labeling in 3D cultured PANC-1 spheroids with or without RETSAT under indicated treatments. **K** Experimental setup and treatment schedule of CDX assay. Tumor sizes were detected by IVIS system at day 7 post transplantation, and starting Gemcitabine treatment at dose of 50 mg/kg weekly and ending at day 28, the mice were monitored until day 49. **L** Representative images of bioluminescence signals in mice bearing with PANC-1 cell derived xenografts. **M, N** Image of cell derived xenografts (**M**) and weight quantification (**N**) from PANC-1 parental and *RETSAT* knockout cells after gemcitabine therapy. **O** Survival curve of mice bearing with PANC-1 cell derived xenografts under indicated therapy. The figure shows the Kaplan–Meier survival curves ($n=5$ biologically independent mice per group). **P** Definition of tumor central and marginal sectors. **Q–S** Representative images (**Q**) and quantification of Ki67 (**R**) and cleaved caspase 3 (**S**) immunohistofluorescence in CDXs central and marginal sectors, respectively. Scale bar = 200 μ m in (**A**), 50 μ m in (**B**), 100 μ m in (**I**) and (**Q**). $n=3$ independent experiments unless otherwise stated. All data are presented as mean \pm SEM. P values were calculated using a two-tailed student's t test

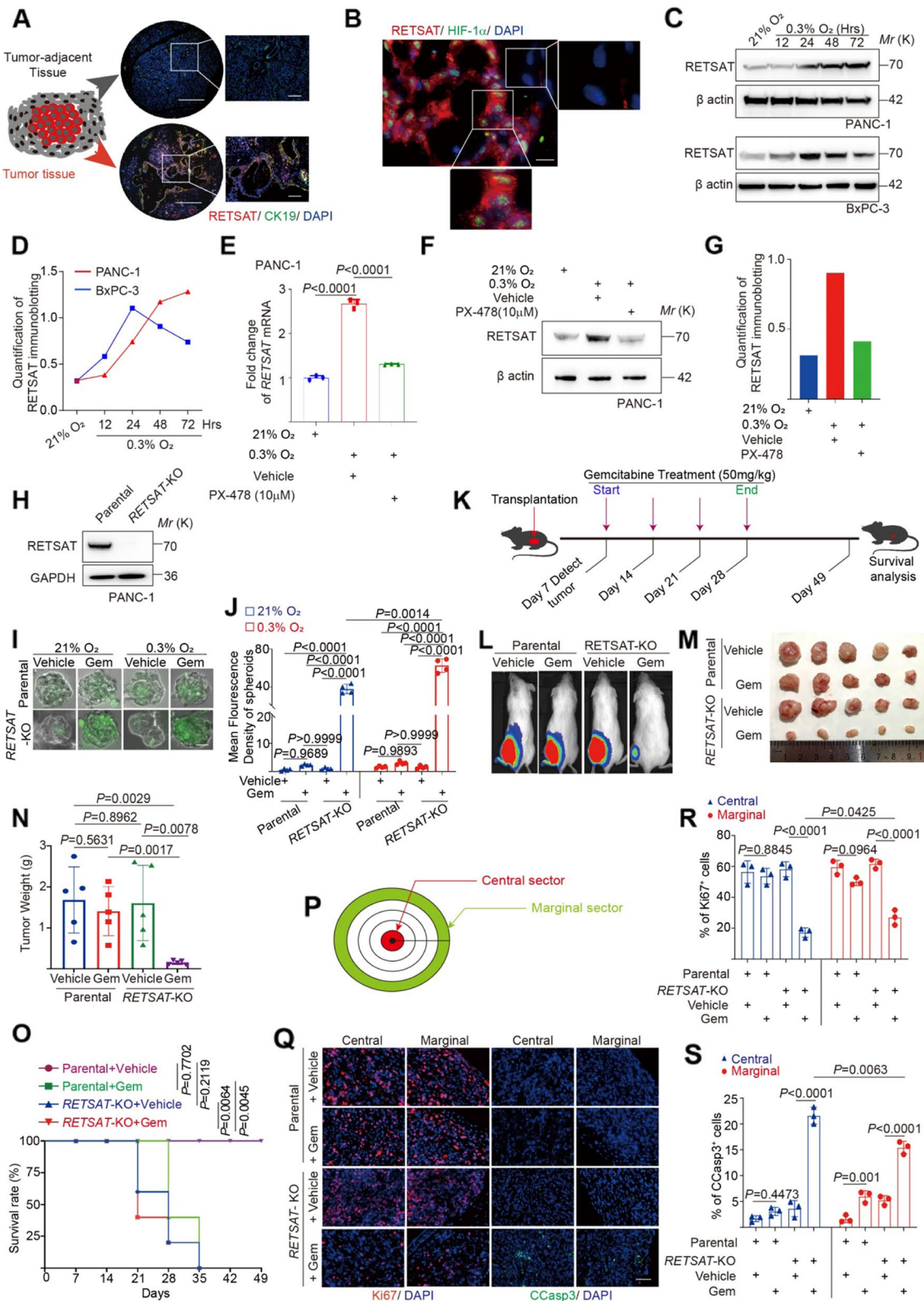


Fig. 2 (See legend on previous page.)

Xenografts were then fixed for immunohistochemistry (IHC) analysis. Central regions are defined as extreme hypoxia sectors of solid tumors where impede efficient PDAC chemotherapy [52]. Based on the diameter of each tumor, we defined the inner 10% area as central sector, and the outer 10% area as marginal sector (Fig. 2P). We used anti-Ki67 antibody to detect proliferating cells, and anti-cleaved caspase 3 (CCasp3) antibody to detect apoptosis. Regarding cell proliferation, there was no difference in parental central sectors ($P=0.8845$ Fig. 2Q-R), and a bit decrease in parental marginal sectors but without statistical significance ($P=0.0964$ Fig. 2Q-R), while in *RETSAT* knockout tissues, *RETSAT* deletion caused dramatic decrease of cell proliferation in both central and marginal sectors of CDXs ($P<0.0001$ Fig. 2Q-R), and central sectors contained less proliferating cells compared to their own marginal counterparts ($P=0.0425$ Fig. 2Q-R). Notably, In terms of apoptosis, *RETSAT* knockout CDXs contained more apoptotic cells in both central and marginal sectors of CDXs ($P<0.0001$), with more apoptotic cells in central regions ($P=0.0063$ Fig. 2Q-S). Together, we concluded that *RETSAT* knockout sensitized PDAC cells to apoptosis in gemcitabine treatment.

RETSAT promotes fork restarting under replication stress

Our in vitro and in vivo results consistently revealed that *RETSAT* knockout sensitized PDAC cells to gemcitabine induced apoptosis under severe hypoxia. We next sought to explore the mechanism. To this goal, we performed immunofluorescence in PDAC cells first to check the subcellular localization of *RETSAT*. In PANC-1 cells, *RETSAT* localized in both cytoplasm and nuclear (Supplementary Fig. 2A), consistent to published study [26]. After 0.2% Triton X-100/PBS pre-wash before paraformaldehyde fixation, cytoplasmic and dissociative *RETSAT* proteins were released. Then we observed that the remaining *RETSAT* showed as minor foci in nuclear morphologically (Fig. 3A). We first hypothesized these

RETSAT foci might be correlated with telomere, since telomere always exhibits as small foci in the cellular nuclei when performing telomeric fluorescence in situ hybridization (T-FISH) assay [53]. However, we observed negative co-localization between telomeres and *RETSAT* foci in anti-*RETSAT* immunofluorescence combined with T-FISH assay (Supplementary Fig. 2B). Next, we tested the correlation of *RETSAT* with another form of minor foci named DNA replication foci when performing BrdU pulse labeling [40]. Obviously, *RETSAT* showed almost 100% co-localization with replication foci in PANC-1 (Fig. 3A) and BxPC-3 (Supplementary Fig. 2C) cell lines. Neither hydroxyurea (HU) induced replication stress nor severe hypoxia (0.3% oxygen tension) changed this co-localization (Supplementary Fig. 2C-E), indicating a constitutive manner of *RETSAT* on DNA replication sites.

iPOND (isolate proteins on nascent DNA) assay allows to examine proteins associated with replicating and newly synthesized DNA in mammalian cells, based on EdU pulse labeling of nascent DNA and covalent cross-link to Biotin through Cu^{II} catalyzed click chemistry reaction. Biotin linked nascent DNA fragments can be enriched by streptavidin-based affinity purification [41]. To confirm *RETSAT* is a fork associated protein, we performed iPOND assay in PANC-1 cells. PCNA was included as a positive control. After immunoblotting of iPOND samples, we clearly observed that *RETSAT* was pulled down from nascent DNA (Fig. 3B). Together, we concluded that *RETSAT* is a fork binding protein. Notably, under hydroxyurea (HU) or gemcitabine induced replicative stress [54], the protein level of *RETSAT* did not increase in PANC-1 cells (Supplementary Fig. 2F-G).

We investigated the correlation between gemcitabine induced DNA damage and fork restarting. To this goal, PANC-1 cells were pulse labeled with IdU for 20 minutes, then treated with 50 nM gemcitabine for 1, 2, 3 and 4 hours, respectively. Cells at each time point were

(See figure on next page.)

Fig. 3 *RETSAT* promotes fork restarting under replication stress. **A** Co-immunostaining of *RETSAT* (green) and BrdU pulse labeled replication foci (red) in PANC-1 cells cultured under normoxia (21% O_2) or hypoxia (0.3% O_2). **B** iPOND assay to validate location of *RETSAT* on replication forks. PCNA was included as a positive control. **C** Immunoblotting of *RETSAT* in PANC-1 and BxPC-3 infected with or without *RETSAT* CRISPR gRNA lentivirus. β actin was used as a loading control. **D, E** Representative images (**D**) and quantification (**E**) of fork restarting in parental or *RETSAT*-KO PANC-1 cells under indicated treatments. 2.5 mM Hydroxyurea (HU) was used to induce replication stress. At least 200 single forks were calculated in each sample. **F, G** Representative images (**F**) and quantification (**G**) of replication fork damage in PANC-1 parental and *RETSAT*-KO cells under indicated treatments. Pulse labeled BrdU foci was indicating DNA replication sites. $\gamma\text{H2A.X}$ was used to indicate DNA damage. **H, I** Immunoblotting of $\gamma\text{H2A.X}$ in parental and *RETSAT*-KO PANC-1 (**H**) and BxPC-3 (**I**) under indicated treatments. β actin was used as a loading control. **J** Quantification of neutral comet assay in parental and *RETSAT*-KO PANC-1 cells under indicated treatments. At least 150 single comets were calculated in each sample. **K** Immunoblotting of ATR, p-ATR (Ser428), CHK1, p-CHK1 (Ser345) and β actin in parental and *RETSAT*-KO PANC-1 cells under indicated treatments. **L** Flow cytometry based Annexin V apoptosis quantification in parental and *RETSAT*-KO PANC-1 cells under indicated treatments. 1 μM PF-47736 was used to inhibit CHK1 activity. **M, N** Representative images (**M**) and quantification (**N**) of clone formation assay of parental or *RETSAT*-KO PANC-1 cells under indicated treatments. Scale bar = 10 μm in (**A**), 50 μm in upper four panels and 10 μm in lowest panel in (**F**). $n=3$ independent experiments unless otherwise stated. All data are presented as mean \pm SEM. P values were calculated using a two-tailed student's t test

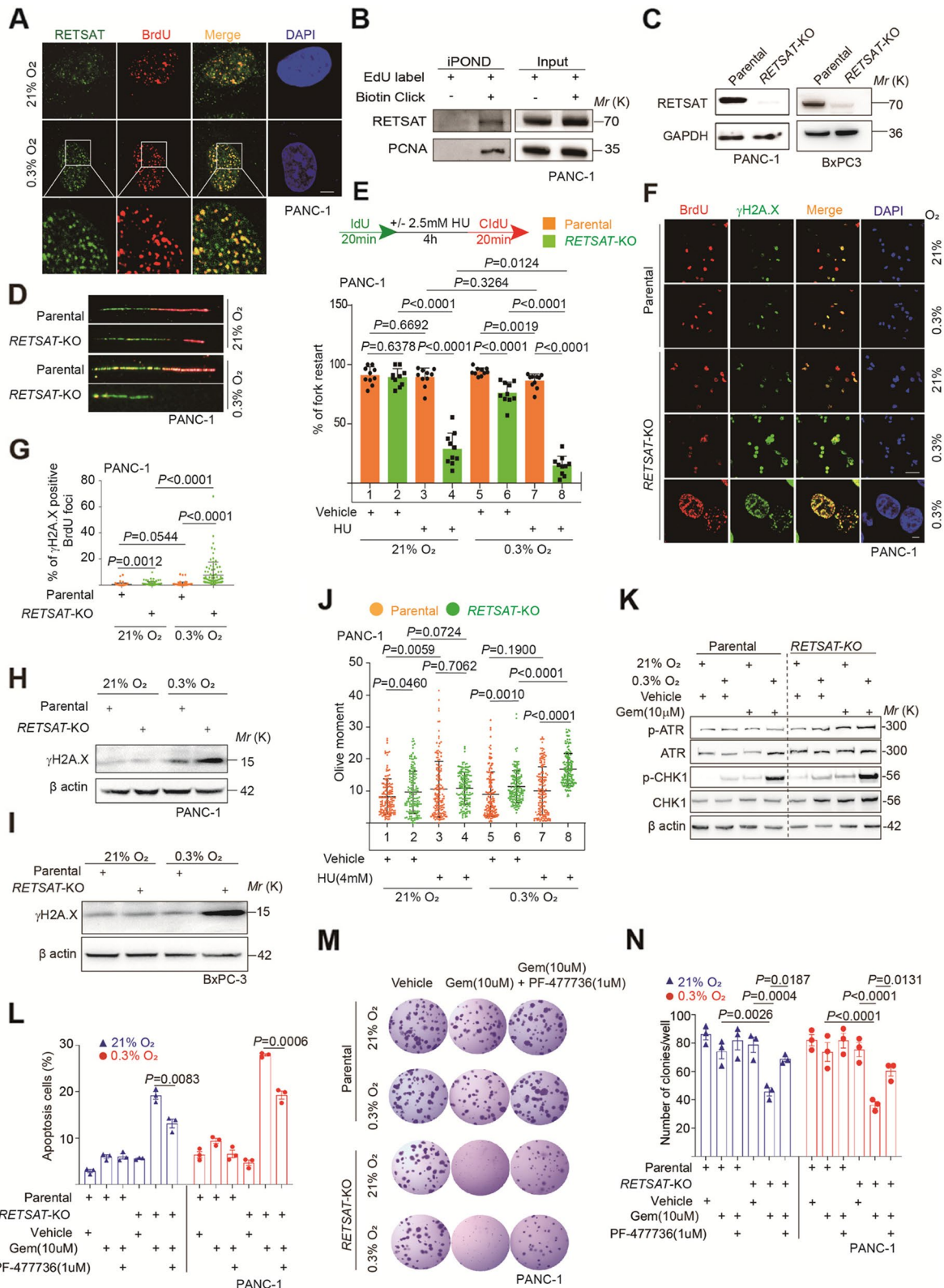


Fig. 3 (See legend on previous page.)

labeled with CldU for 20 minutes, and collected for neutral comet assay (to examine double-strand DNA damage) and DNA fiber assay (to examine fork restarting) in parallel (Supplementary Fig. 2H). The levels of DNA damage and efficiency of fork restarting were quantified and normalized by the control value (control sample with vehicle but without Gem treatment). In the process of gemcitabine treatment, fork restarting efficiency decreased gradually, while the levels of DNA damage increased dramatically, reminding that fork restarting deficiency could contribute to DNA damage accumulation (Supplementary Fig. 2I). Indeed, when using cells at 4 hours post gemcitabine treatment for immunostaining, we observed dramatic co-localization of CldU and γ H2A.X (Supplementary Fig. 2J), highlighting DNA damage occurred at fork restarting sites.

We next sought to determine the functions of *RETSAT* in replication fork dynamics. *RETSAT* deletion was achieved using CRISPR mediated gene knockout technology in PANC-1 and BxPC-3 cells (Fig. 3C). DNA fiber assay is a valuable method to evaluate many aspects of DNA replication at single fork resolution, e.g. fork velocity, nascent DNA stability and stalled fork restart [55]. The treatment of 2.5 mM HU for 4 hours dramatically impaired fork velocity and nascent DNA stability, indicating that the dosage of HU could induce replication stress successfully. We found that *RETSAT* knockout did not change fork velocity ($P=0.1377$ Supplementary Fig. 2K) or nascent DNA stability ($P=0.2965$ Supplementary Fig. 2L). Then we focused on fork restarting. Under normoxia (21% O₂), treatment of 2.5 mM HU for 4 hours had no influence on fork restarting in parental cells ($P=0.6692$ between 1st and 3rd bars), while the same treatment significantly decreased fork restarting under severe hypoxia (0.3% O₂) ($P=0.0019$ between 5th and 7th bars, Fig. 3D-E), indicating a synergically detrimental efforts of HU and hypoxia on fork restarting. *RETSAT*-KO cells showed much worse fork restarting under HU treatment ($P<0.0001$ between 2nd and 4th bars), or severe hypoxia condition ($P<0.0001$ between 5th and 6th bars). Notably, under co-induced stresses from HU and severe hypoxia, parental cells could maintain fork restarting ($P=0.3264$ between 3rd and 7th bar), while *RETSAT*-KO cells got further decreased efficiency of fork restart ($P=0.0124$ between 4th and 8th bar) (Fig. 3E). Together, we concluded *RETSAT* promotes fork restarting under replication stress.

BLM and SMARCAL1 are two key factors of fork restarting machinery [56, 57]. To investigate the importance of fork restarting system in gemcitabine resistance of PDAC cells, we knocked down these two factors in PANC-1 gemcitabine resistant (PANC-1/Gem-R) line, respectively (Supplementary Fig. 3A-B). Each gene was

targeted using two different short hairpin RNAs. Under 50 nM gemcitabine induced replication stress, PANC-1/Gem-R cells were more efficiently to restart stalled forks ($P<0.0001$, grey region in Supplementary Fig. 3C), and resistant to gemcitabine induced apoptosis ($P<0.0001$, grey region in Supplementary Fig. 3E) than parental counterpart, emphasizing the correlation of fork restarting abilities and gemcitabine resistance. Consistent to published results [56, 57], knocking down either *BLM* or *SMARCAL1* decreased fork restarting efficiency significantly (yellow region in Supplementary Fig. 3C). Correspondingly, when performing flow cytometry based apoptotic analysis, we found dramatically increased apoptosis in *BLM* or *SMARCAL1* knocking down cells compared to shRNA vector control ($P<0.0001$, yellow region in Supplementary Fig. 3D-E), indicating that PANC-1/Gem-R cells lost gemcitabine resistance when fork restarting machinery were disturbed. We concluded from these results that fork restarting system is crucial for PDAC cells resistant to gemcitabine.

Persistent stalling forks are prone to transform into DNA breaks consequently, which causes DNA damage accumulation and genomic instability [58]. Consistently, both immunostaining (Fig. 3F-G) and immunoblotting (Fig. 3H-I) using DNA damage marker γ H2A.X revealed drastically higher level of DNA breaks in *RETSAT*-KO compared to parental. Notably, almost all γ H2A.X foci co-localized with BrdU positive site in *RETSAT*-KO cells, further supporting the DNA breaks were derived from stalled forks predominantly (zoomed panel in Fig. 3F). Consistently, when performing neutral comet assay to evaluate DNA damage, we found that accumulated DNA double strand breaks in *RETSAT*-KO cells under HU and severe hypoxia combined stresses ($P<0.0001$ between 7th and 8th groups) (Fig. 3J).

Over threatened by replication stress and DNA damage predominantly initiates ATR-CHK1 signaling induces apoptosis [59]. We next sought to find out the determinants behind apoptotic sensitivity of *RETSAT* knockout cells in response to such stresses. Immunoblotting results revealed that the levels of both active ATR (phosphorylation at serine 428) and active CHK1 (phosphorylation at serine 345) were higher in *RETSAT*-KO cells compared to parental (Fig. 3K), indicating over-activated ATR-CHK1 signaling in *RETSAT*-KO cells. When treated cells with CHK1 antagonist PF-477736 [60] (1 μ M for 72 hours), we found PF-477736 could dramatically relieve apoptosis in *RETSAT*-KO cells ($P=0.0006$ Gem and PF-477736 combined group versus Gem single treated group under 0.3% O₂, Fig. 3L). Consistently, the colony formation ability of *RETSAT*-KO cells was partially rescued as well (Fig. 3M-N). These results indicated that CHK1 signaling

promotes apoptosis in *RETSAT* knockout PDAC cells under replication stress.

RETSAT recruits DDX39B onto replication forks to resolve R-loop

Based on the functional analysis of *RETSAT* in fork restarting, we next sought to examine the proteomic changes of replisome with or without *RETSAT* to find out its molecular mechanisms. To this goal, we performed iPOND combined with LC-MS/MS screening in parental and *RETSAT*-KO PANC-1 cells (Fig. 4A and Supplementary Fig. 4A). The cells were treated with vehicle (DMSO) (sample 2 and 3) or gemcitabine (sample 4 and 5) to induce replication stress. Meanwhile, the parental PANC-1 with EdU labeling but without Biotin click (sample 1) was set up as a non-specific binding control. The proteins identified in sample 1 were defined as non-specific and excluded from the rest samples (Supplementary Table 1). Under normal cultural conditions, we identified 32 proteins missing from *RETSAT*-KO forks and 9 proteins newly emerged in *RETSAT*-KO sample compared to parental (Supplementary Fig. 4B-C and Supplementary Table 2). Under gemcitabine induced replication stress conditions, 19 proteins were absent from in *RETSAT*-KO sample, and 14 proteins were newly emerged (Supplementary Fig. 4D-E and Supplementary Table 3).

We overlapped subgroups of absent proteins in *RETSAT*-KO samples under either normal cultured (32 proteins in Supplementary Fig. 4B) or gemcitabine induced replication stress conditions (19 proteins in Supplementary Fig. 4D). Five proteins including DDX39B, HNRNPA3, RDX, PGK1 and RPL30 were identified as shared missing members in *RETSAT*-KO samples (Supplementary Fig. 4B and D, highlighted in red). Since we have confirmed the functions of *RETSAT* in DNA replication and genomic stability, we further overlapped these five proteins with the dataset of DNA damage response genes (Supplementary Table 4) (downloaded from [http://](http://amigo.geneontology.org)

amigo.geneontology.org). Finally, only one protein named DDX39B was screened out (Fig. 4B-C).

DDX39B (also named as UAP56 or BAT1) is a DEAD-box family helicase and plays pivotal roles in mRNA binding, splicing, and export [61]. In the process of DNA replication, DDX39B is responsible for unwinding R-loops to avoid collisions between DNA replication machinery and unresolved R-loops, finally save genomic stability [22, 62]. We first performed co-immunostaining assay to examine the location of R-loop and DNA damage sites. As shown in Supplementary Fig. 5A, significant co-localization of R-loop and γ H2A.X foci in PANC-1 cells under gemcitabine treatment. When ectopically expressed RNase H1 in PANC-1 cells (Supplementary Fig. 5B), the overall DNA damage levels in gemcitabine treated group was downregulated dramatically (Supplementary Fig. 5C-D), highlighting R-loop is involved in gemcitabine induced DNA damage.

To investigate the functions of DDX39B in gemcitabine resistance, we knocked down *DDX39B* in PANC-1/Gem-R cells. Western blotting was performed to confirm knocking down efficiency (Supplementary Fig. 5E). Compared with shRNA vector control, the capacities of in vitro proliferation (Supplementary Fig. 5F-G) and colony formation (Supplementary Fig. 5H-I) were dramatically decreased in PANC-1/Gem-R cells. Notably, PANC-1/Gem-R cells without efficient DDX39B expression were sensitive to gemcitabine induced apoptosis (Supplementary Fig. 5J). These results highlighted the importance of DDX39B in gemcitabine resistance of pancreatic cancer cells.

We isolated nuclear protein lysis of PANC-1 cells and confirmed the interaction of *RETSAT* and DDX39B under gemcitabine treatment or severe hypoxia using co-immunoprecipitation assay (Fig. 4D and Supplementary Fig. 5K). Immunoblotting results revealed that *RETSAT* knockout did not change the total abundance of DDX39B, and *vice versa* (Supplementary Fig. 5L-M). When examining subcellular localizations, we found that

(See figure on next page.)

Fig. 4 *RETSAT* recruits DDX39B onto replication forks to resolve R-loop. **A** Treatment and sample collections used for iPOND combined with LC-MS/MS detection. **B** Overlapping analysis between absent proteins in *RETSAT*-KO groups and DNA damage response protein dataset. **C** Heatmap of DDX39B based on its abundance in LC-MS/MS results. **D** Co-immunoprecipitation using anti-*RETSAT* antibody combined with immunoblotting to confirm the interaction of *RETSAT* and DDX39B in PANC-1 cells under indicated treatments. GAPDH was included as a negative control. **E** Co-immunostaining of DDX39B (green) and pulse labeled BrdU (red) in parental and *RETSAT*-KO PANC-1 cells. **F** Immunoblotting of DDX39B in nuclear and cytoplasmic extractions of PANC-1 cells with or without *RETSAT*. GAPDH and H2B were used as a cytoplasmic and nuclear loading control respectively. **G** iPOND combined with immunoblotting to examine DDX39B loading dosage on replication forks in parental and *RETSAT*-KO PANC-1 cells. **H, I** Representative images (**H**) and quantification (**I**) of R-loop dot blotting using S9.6 antibody in parental and *RETSAT*-KO PANC-1 cells under indicated treatments. Anti-dsDNA antibody was used as a loading control. **J, K** Representative images (**J**) and quantification (**K**) of R-loop accumulation in parental and *RETSAT*-KO PANC-1 cells under indicated treatments. **L** Dot Blotting of R-loops using S9.6 antibody in parental and *RETSAT*-KO PANC-1 cells with or without RNase H1 ectopic expression. Anti-dsDNA antibody was used as a loading control. **M, N** Representative images (**M**) and quantification (**N**) of γ H2A.X positive BrdU foci in *RETSAT*-KO PANC-1 cells with or without ectopically expression of RNase H1 under indicated cultural conditions. Scale bar = 10 μ m. $n = 3$ independent experiments unless otherwise stated. All data are presented as mean \pm SEM. *P* values were calculated using a two-tailed student's *t* test

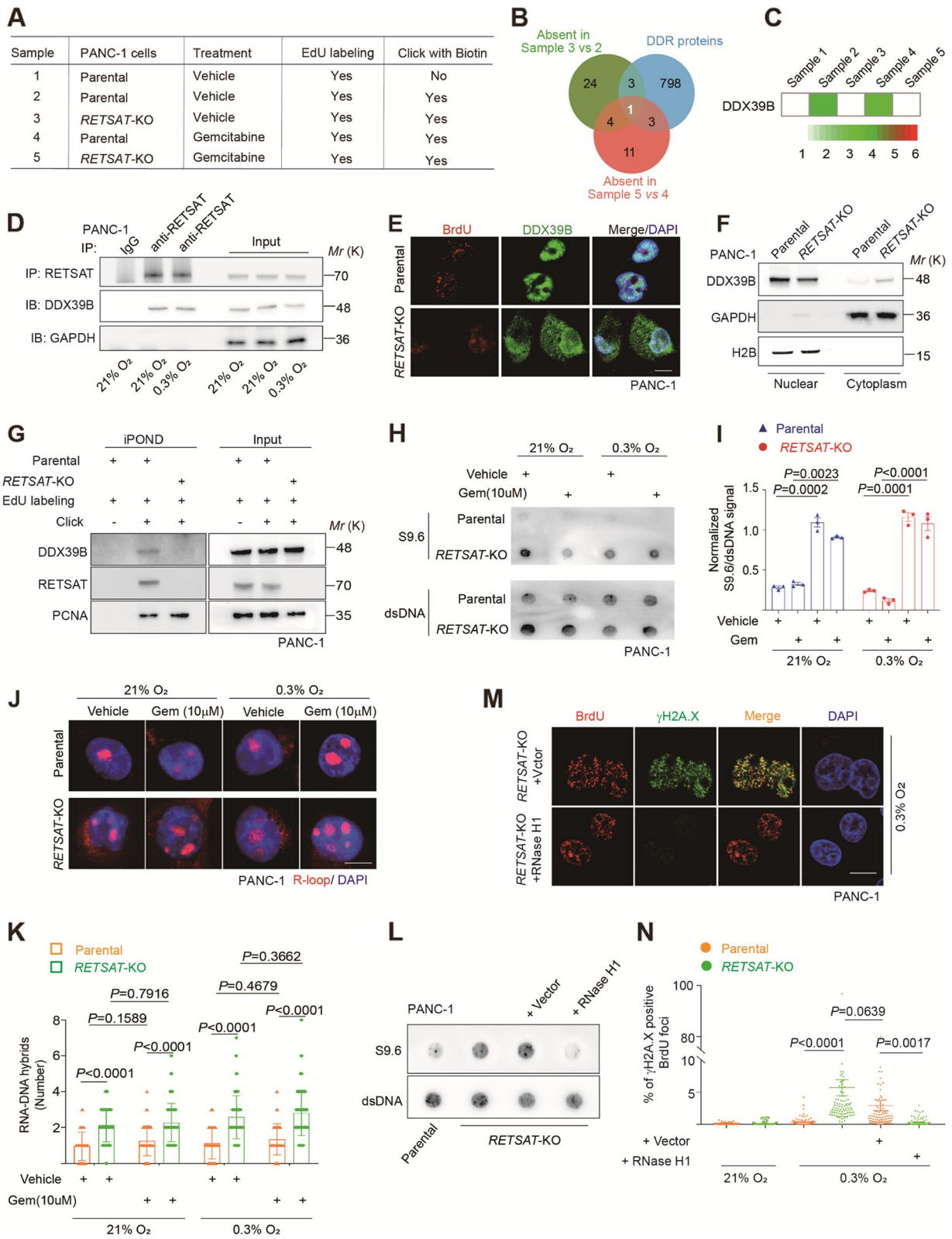


Fig. 4 (See legend on previous page.)

DDX39B knocking down did not change the location of *RETSAT* onto replication foci (Supplementary Fig. 5N). Notably, *DDX39B* locates in nuclear in PANC-1 parental cells (upper panel in Fig. 4E), while we observed significant amounts of *DDX39B* released into cytoplasm in *RETSAT*-KO cells (lower panel in Fig. 4E). We further validated this phenotype using cytoplasm-nuclei separation kit and immunoblotting assay. The results showed that nuclear *DDX39B* was decreased in *RETSAT*-KO cells, while cytoplasmic *DDX39B* was dramatically increased correspondingly (Fig. 4F), further supporting our observation in immunofluorescence assay (Fig. 4E). *DDX39B* functions to resolve R-loops on the whole chromatin level [22]. Especially, we confirmed the loading of *DDX39B* on forks was dramatically decreased without *RETSAT* by using iPOND assay (Fig. 4G).

To validate fork restarting defects in *RETSAT*-KO cells was caused by R-loop accumulation, we performed R-loop dot blotting (Fig. 4H-I) and immunofluorescence (Fig. 4J-K) using S9.6 antibody, and confirmed overwhelming R-loops in *RETSAT*-KO PANC-1 cells. When ectopically expressed RNase H1 in *RETSAT*-KO cells (Supplementary Fig. 5O), the overwhelmed R-loops were efficiently resolved in *RETSAT*-KO cells (Fig. 4L), although abundant *DDX39B* still existed in cytoplasm (Supplementary Fig. 5P). As such, we observed dramatic decrease of γ H2AX positive replication foci in *RETSAT*-KO cells even under severe hypoxia (Fig. 4M-N). Together, we concluded that *RETSAT* is responsible for recruitment of *DDX39B* onto forks, through which resolves R-loop obstacle and saves fork stability.

Evaluation of synergetic effects of *DDX39B* inhibitor CCT018159 and gemcitabine in human PDAC organoids system

The association of *RETSAT* and *DDX39B* is crucial for fork restarting and genomic stability. Knocking out *RETSAT* in PANC-1 sensitized cells to gemcitabine induced apoptosis (Fig. 2). Notably, knocking down *DDX39B* exhibited similar apoptotic phenotype under either 20% or 0.3% oxygen tensions (Fig. 5A, Supplementary Fig. 5M), highlighting the two proteins to be druggable targets for PDAC chemotherapy.

DDX39B unwinds R-loop relying on its ATPase activity, because it has been confirmed that *DDX39B* -K95A and -E197A mutants that defective for the ATPase activity could not unwind R-loop [22]. Notably, CCT018159, originally identified as a heat shock protein 90 (HSP90) inhibitor [63], was found to be able to inhibit the ATPase activity of *DDX39B* in antiviral study [64]. We wondered the possibility of CCT018159 in PDAC chemotherapy. To this goal, we derived two PDAC organoid lines

from surgery tumor tissues following standard protocol (Fig. 5B) [46–48]. The organoids were treated with vehicle, 25 nM gemcitabine, 10 μ M CCT018159 or combined together and cultured under 20% or 0.3% oxygen tensions for 72 hours. Organoids were labeled with green-fluorescent caspase 3/7 probe (Fig. 5C and E), or stained with FITC Annexin V for flow cytometry analysis to evaluate apoptosis (Fig. 5G). In both organoid lines, CCT018159 performed better than gemcitabine under both oxygen tensions ($P < 0.0001$ Gem versus CCT018159 Fig. 5D, F, H, I). Combined treatment showed significantly synergistic effects, with statistical significance and much stronger green fluorescence in combined groups (Fig. 5D, F, H, I).

Discussion

Here we report that *RETSAT* gene plays key roles in TME hypoxia adaptation and gemcitabine chemotherapy in the context of pancreatic ductal carcinoma (PDAC). Our study demonstrates that *RETSAT* is a fork associated protein in the nuclear. HIF-1 α signaling promotes the expression of *RETSAT* upstream. *RETSAT* interacts with *DDX39B*, and recruits *DDX39B* onto replication forks to resolve R-loops and avoids collisions between DNA replication and transcription machineries, through which saves fork restarting and avoids fork damage initiated CHK1 activation and apoptosis. However, there are a few limitations in our study. Although we focus on the nuclear functions of *RETSAT*, *RETSAT* has been well defined as an oxidoreductase in the cytoplasm that catalyzes retinol into 13,14-dihydroretinol, we cannot formally exclude the possibility that other mechanisms may also directly or indirectly contribute to the phenotypes of this study. Additionally, we did not confirm the interactions of *RETSAT* with other proteins we identified through iPOND-MS. We studied the synergic effects of CCT018159 and gemcitabine in PDAC organoids system. However, CCT018159 is developed to be an antagonist of HSP90. Recently, it was revealed that CCT018159 has inhibition effects to *DDX39B*. So CCT018159 is not a selective antagonist targeting *DDX39B*. Meanwhile, HSP90 has been reported to play multiple roles in pancreatic cancers, e.g. chromosome stability [65], JAK/STAT and MAPK signaling [66], we did not exclude the participation of HSP90 in our study. Regardless, this dataset demonstrates that enhancing fork damage and CHK1 signaling through targeting R-loop helicase can be explored for sensitizing pancreatic cells to gemcitabine. We anticipate our findings to have far-reaching implications for developing future combinatory therapeutics of pancreatic cancer. So far, there is no selective antagonists available targeting *RETSAT* or *DDX39B*. To achieve this goal, drug development targeting *RETSAT* and *DDX39B* specifically will be key works needed to be addressed.

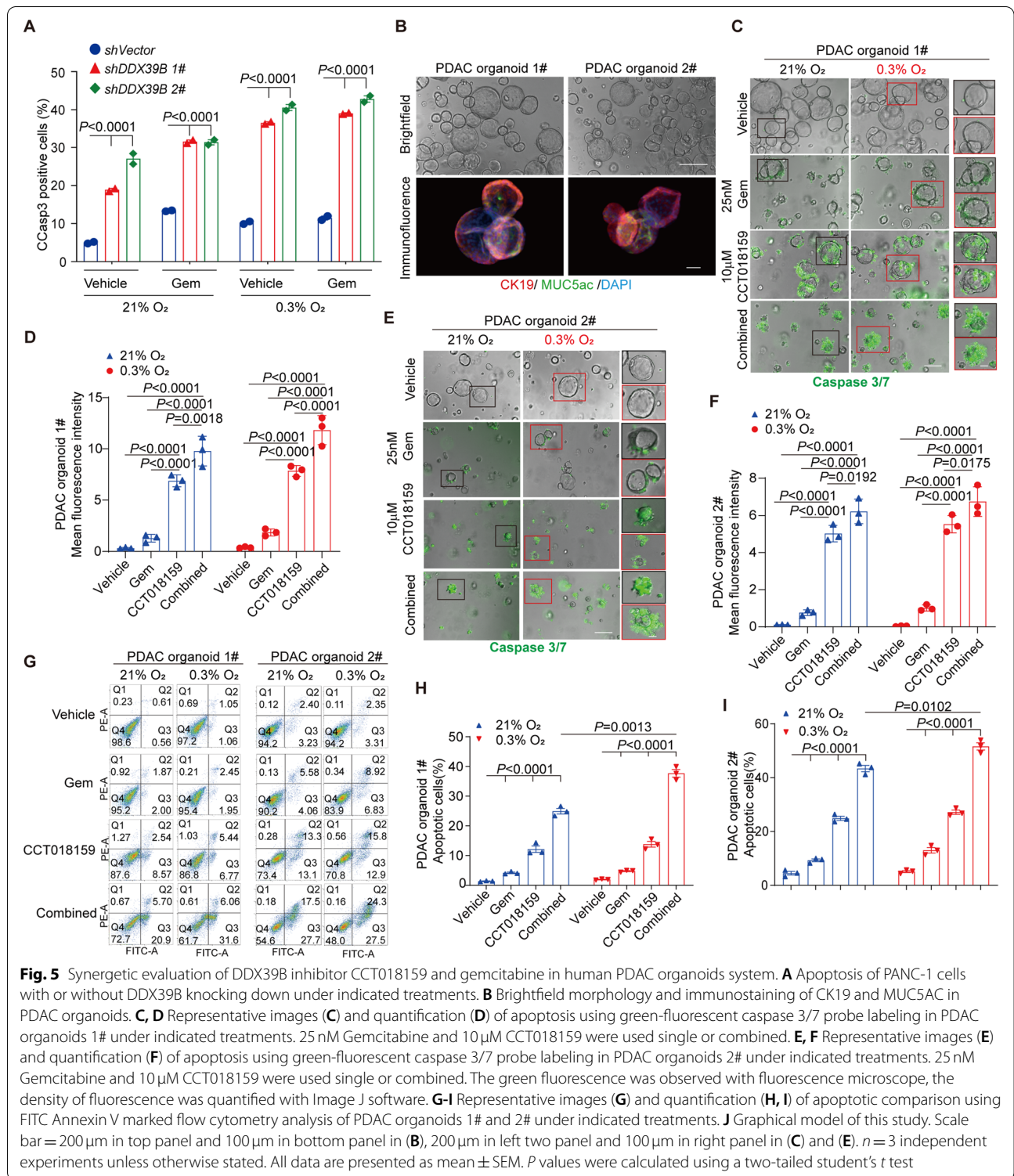
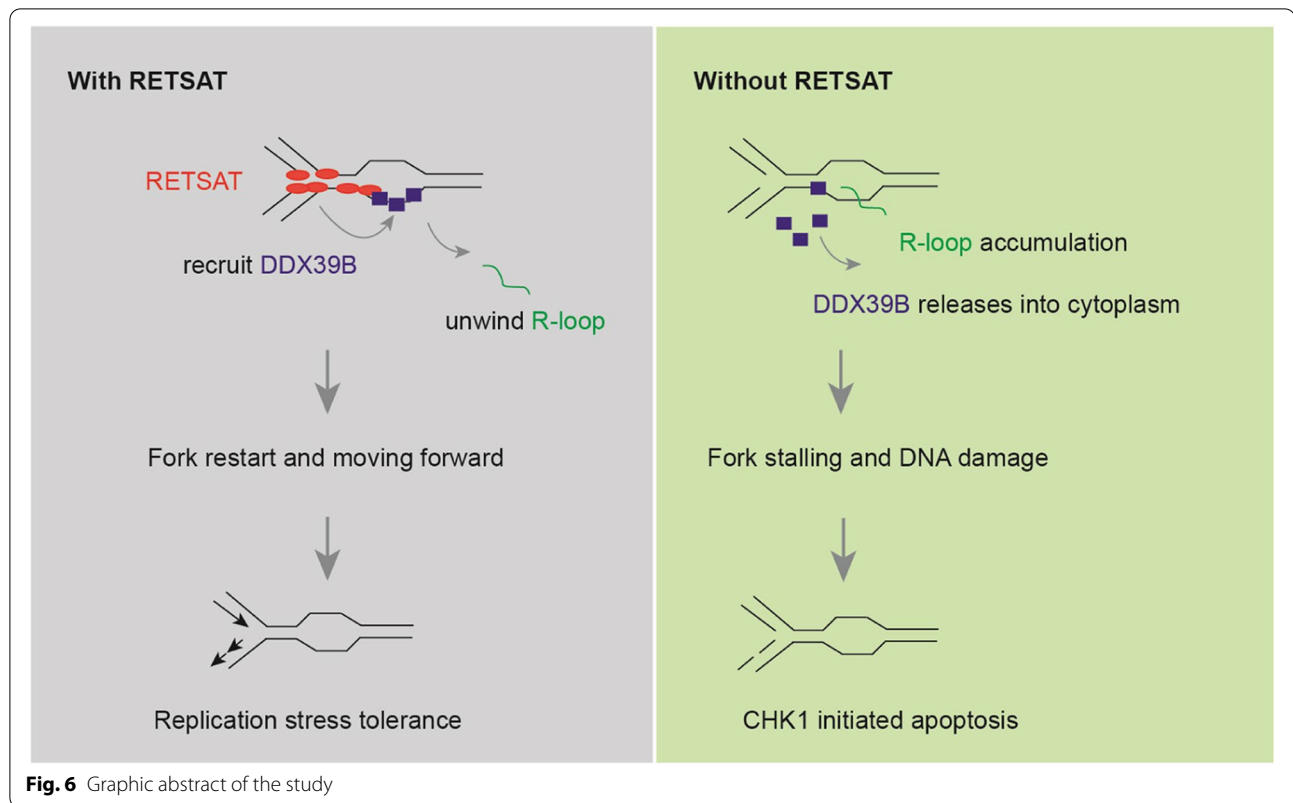


Fig. 5 Synergetic evaluation of DDX39B inhibitor CCT018159 and gemcitabine in human PDAC organoids system. **A** Apoptosis of PANC-1 cells with or without DDX39B knocking down under indicated treatments. **B** Brightfield morphology and immunostaining of CK19 and MUC5ac in PDAC organoids. **C, D** Representative images (**C**) and quantification (**D**) of apoptosis using green-fluorescent caspase 3/7 probe labeling in PDAC organoids 1# under indicated treatments. 25 nM Gemcitabine and 10 µM CCT018159 were used single or combined. **E, F** Representative images (**E**) and quantification (**F**) of apoptosis using green-fluorescent caspase 3/7 probe labeling in PDAC organoids 2# under indicated treatments. 25 nM Gemcitabine and 10 µM CCT018159 were used single or combined. The green fluorescence was observed with fluorescence microscope, the density of fluorescence was quantified with Image J software. **G-I** Representative images (**G**) and quantification (**H, I**) of apoptotic comparison using FITC Annexin V marked flow cytometry analysis of PDAC organoids 1# and 2# under indicated treatments. **J** Graphical model of this study. Scale bar = 200 µm in top panel and 100 µm in bottom panel in (**B**), 200 µm in left two panel and 100 µm in right panel in (**C**) and (**E**). *n* = 3 independent experiments unless otherwise stated. All data are presented as mean ± SEM. *P* values were calculated using a two-tailed student's *t* test

Our immunofluorescence results revealed tremendous co-localization of RETSAT and BrdU pulse labeled replication foci. However, in the peptide list identified from iPOND combined with mass spectrometry

analysis, we got no RETSAT peptides. When performing iPOND combined with immunoblotting to detect RETSAT, we found it was uneasy to detect RETSAT following standard iPOND procedure. We had to



synchronize cells into S phase in order to purify replication forks as many as possible, then we were able to detect bands of RETSAT in immunoblotting. Based on our experiences in the previous study, classical fork binding proteins such as PCNA or RPAs could be easily detected in iPOND assay [40]. Compared with them, the abundance of RETSAT on replication forks might be low. This phenomenon might be useful to understand the biological characters of RETSAT protein more detailedly.

In our previous study, we have identified *RETSAT* as a convergent gene in high-altitude mammal species, emphasizing the contribution of *RETSAT* in mammalian hypoxia adaptation [32]. Here we report its functions in pancreatic cancer cells. This indicates the possible conservation of hypoxia adaptation between high-altitude mammals and solid tumor cells. Our study demonstrated that translating mammalian genetic resources in high-altitude adaption into oncological hypoxia research might be an alternative avenue towards precision tumor therapy.

Conclusions

In this study, we identified RETSAT to be a novel replication fork protein. Hypoxia upregulates RETSAT expression. RETSAT interacts with DDX39B in order to resolve

R-loops and avoid collisions occurred between replication forks and transcriptional machinery, through which finally promotes fork restarting and endows PDAC cells resistant to gemcitabine chemotherapy. Our study highlighted the importance of RETSAT mediated fork restarting mechanisms in hypoxia adaptation and gemcitabine resistance of PDAC, and provided CCT018159 to be a useful chemical in PDAC chemotherapy. In summary, these findings shed light on novel molecular mechanisms and provide new insight into developing effective therapeutic strategies for pancreatic ductal adenocarcinoma (Fig. 6).

Abbreviations

PDAC: Pancreatic ductal adenocarcinoma; PANC-1/Gem-R: Gemcitabine resistant PANC-1 subline cell; CDX: Cell derived xenograft; KO: Knockout; T-FISH: Telomeric fluorescence in situ hybridization; iPOND: Isolate proteins on nascent DNA; HU: Hydroxyurea; Gem: Gemcitabine; TME: Tumor microenvironment; RNR: Ribonucleotide reductase; BrdU: Bromodeoxyuridine; EdU: 5-ethynyl-2'-deoxyuridine; IdU: 5-Iodo-2'-deoxyuridine; CldU: 5-chloro-2'-deoxyuridine; HCl: Hydrochloric acid; EDTA: Ethylene diamine tetraacetic acid; PBS: Phosphate buffer solution; DMSO: Dimethylsulfoxide; BSA: Bovine serum albumin; SDS: Sodium dodecyl sulfate; HPLC: High performance liquid chromatography; FDR: False discovery rates; Co-IP: Co-immunoprecipitation; TCGA: The Cancer Genome Atlas; IHC: Immunohistochemistry; FPKM: Fragments per kilobase million; qRT-PCR: Quantitative real-time PCR; CCasp3: Cleaved caspase 3; LC-MS/MS: Liquid Chromatograph Mass Spectrometer; BLM: Blooms Syndrome; SMARCAL1: SWI/SNF related, matrix associated, actin dependent regulator of chromatin, subfamily a like 1.

Supplementary Information

The online version contains supplementary material available at <https://doi.org/10.1186/s13046-022-02490-3>.

Additional file 1: Supplementary Fig. 1. *RETSAT* deletion sensitizes PDAC cells to gemcitabine. (A) The expression of *RETSAT* in *KRAS* mutant ($n=86$) and *KRAS* wild type ($n=10$) PDAC tumor tissues from TCGA database. (B, C) Immunostaining (B) and quantification (C) of cell proliferation marker Ki67 in parental and *RETSAT*-KO PANC-1 cells with or without gemcitabine treatment. (D, E) Immunostaining of cleaved caspase 3 (D) and flow cytometry based Annexin V apoptosis quantification (E) in parental and *RETSAT*-KO PANC-1 cells with or without gemcitabine treatment under 21% O₂ or 0.3% O₂. (F, G) Images (F) and quantification (G) of flow cytometry based Annexin V apoptosis of 3D culture PANC-1 spheroids under indicated treatments. (H, I) Images (H) and quantification (I) of *in vivo* bioluminescence of all mice at indicated time. (J-M) Bioluminescence quantifications of each group including parental with Vehicle (J), *RETSAT*-KO with Vehicle (K), parental with Gem (L), *RETSAT*-KO with Gem (M) were shown. Scale bar = 100 μ m. $n=3$ independent experiments unless otherwise stated. All data are presented as mean \pm SEM. *P* values were calculated using a two-tailed student's *t* test. **Supplementary Fig. 2.** *RETSAT* localizes onto DNA replication forks and has no effects on fork velocity or nascent DNA stability. (A) Immunofluorescence of *RETSAT* in PANC-1 cells with or without 0.2% Triton X-100 pre-wash ahead of paraformaldehyde fixation. (B) Co-immunostaining of *RETSAT* and telomeric PNA probe in BxPC-3 cells. (C, D) Co-immunostaining of *RETSAT* (green) and BrdU pulse labeled replication foci (red) in BxPC-3 and PANC-1 cells cultured under vehicle or HU induced stress conditions. (E) Co-immunostaining of *RETSAT* (green) and BrdU pulse labeled replication foci (red) in BxPC-3 cells under 21% or 0.3% O₂ conditions. (F, G) Immunoblotting of *RETSAT* in PANC-1 cells treated with 4 mM HU (F) or 10 μ M gemcitabine (G) at indicated time points. β actin was used as a loading control. (H, I) Experimental setup (H) and quantifications (I) of DNA fiber and neutral comet assay in PANC-1 cells treated with 50 nM gemcitabine at indicated time points. (J) Co-immunostaining of γ H2A.X (green) and CldU labeled fork restarting sites (red) in PANC-1 cells treated with 50 nM gemcitabine. (K) Quantification of fork velocity in parental and *RETSAT*-KO PANC-1 cells with or without HU treatment. At least 200 single forks were calculated in each sample. (L) Evaluation of nascent DNA stability in parental and *RETSAT*-KO PANC-1 cells with or without HU treatment, calculated by ratio of CldU length divided by own IdU length. At least 200 single forks were calculated in each sample. Scale bar = 10 μ m. $n=3$ independent experiments unless otherwise stated. All data are presented as mean \pm SEM. *P* values were calculated using a two-tailed student's *t* test. **Supplementary Fig. 3.** Fork restarting system is crucial for PDAC cells resistant to gemcitabine. (A, B) Immunoblotting of BLM (A) and SMARCAL1 (B) in PANC-1/Gem-R cells transfected with shVector or indicated shRNA lentivirus. β actin was used as a loading control. (C) Quantification of fork restarting in PANC-1 and PANC-1/Gem-R cells with or without BLM and SMARCAL1 knocking down under vehicle or 50 nM gemcitabine treatment. (D, E) Images (D) and quantification (E) of flow cytometry based Annexin V apoptosis of PANC-1 and PANC-1/Gem-R with or without BLM and SMARCAL1 knocking down under vehicle or 10 μ M gemcitabine treatment. $n=3$ independent experiments unless otherwise stated. All data are presented as mean \pm SEM. *P* values were calculated using a two-tailed student's *t* test. **Supplementary Fig. 4.** Changes of replisome components in response to *RETSAT* knocking out using iPOND combined with LC-MS/MS identification. (A) Corresponding to Fig. 4A, schematic of iPOND assay combined with LC-MS/MS analysis. (B) Heatmap of absent proteins in *RETSAT*-KO PANC-1 cells compared with parental under vehicle treatment. (C) Heatmap of newly emerged proteins in *RETSAT*-KO PANC-1 cells compared with parental under vehicle treatment. (D) Heatmap of absent proteins in *RETSAT*-KO PANC-1 cells compared with parental under gemcitabine treatment. (E) Heatmap of newly emerged proteins in *RETSAT*-KO PANC-1 cells compared with parental under gemcitabine treatment. **Supplementary Fig. 5.** *RETSAT* interacts with DDX39B and avoids R-loop accumulation. (A) Co-immunostaining of γ H2A.X (green) and R-loop (red) in PANC-1 cells with or without 10 μ M gemcitabine treatment. S9.6 antibody was used to label R-loop. (B) Immunoblotting of RNase H1 in PANC-1 cells with or without

RNase H1 ectopic expression. β actin was used as a loading control. (C, D) Immunostaining (C) and quantification (D) of γ H2A.X (green) positive PANC-1 cells with or without RNase H1 ectopic expression under indicated treatment. (E) Immunoblotting of DDX39B in PANC-1/Gem-R cells with or without DDX39B knocking down. (F, G) Immunostaining (F) and quantification (G) of Ki67 in PANC-1/Gem-R cells with or without DDX39B knockdown under vehicle or 10 μ M gemcitabine treatment. (H, I) Clone formation (H) and quantification (I) of PANC-1/Gem-R cells with or without DDX39B knocking down under vehicle or 10 μ M gemcitabine treatment. (J) Flow cytometry based Annexin V apoptotic analysis of PANC-1/Gem-R cells with or without DDX39B knockdown under vehicle or 10 μ M gemcitabine treatment. (K) Co-immunoprecipitation using anti-*RETSAT* antibody combined with immunoblotting to confirm the interaction of *RETSAT* and DDX39B in PANC-1 cells under vehicle or gemcitabine treatments. GAPDH was used as a negative control. (L, M) Immunoblotting of *RETSAT* and DDX39B in parental, *RETSAT*-KO and DDX39B knocking down PANC-1 cells. β actin was used as a loading control. (N) Co-immunostaining of *RETSAT* (green) and BrdU pulse labeled replication foci (red) in PANC-1 cells with or without DDX39B under indicated conditions. (O) Immunoblotting of RNase H1 in *RETSAT*-KO PANC-1 cells with or without RNase H1 ectopic expression. β actin was used as a loading control. (P) Immunostaining of DDX39B in parental and *RETSAT*-KO PANC-1 cells with or without RNase H1 ectopic expression. Scale bar = 10 μ m in (A) and (H), 50 μ m in (C) and (F). $n=3$ independent experiments unless otherwise stated. All data are presented as mean \pm SEM. *P* values were calculated using a two-tailed student's *t* test.

Additional file 2.

Additional file 3.

Additional file 4.

Additional file 5.

Acknowledgements

The authors would like to thank animal facility at Kunming Institute of Zoology, Chinese Academy of Sciences for assistance in animal assays.

Authors' contributions

QT, XL, XY, RL, KL, QC, XH, and QC performed cellular and animal experiments. XY and HJ performed iPOND and mass spectrometry detection. RL performed clinical survival investigation of PDAC patients. GL performed statistical analysis. BZ and QT designed the experiments. BZ, PS, HZ, and GX supervised the studies. BZ and QT wrote the paper. BZ conceived the study. The author(s) read and approved the final manuscript.

Funding

This study was supported by National Key Research & Developmental Program of China (2021YFA0805701 to BZ), the Applied Basic Research Programs of Science and Technology Commission Foundation of Yunnan Province (202101AS070149 to BZ), the National Natural Science Foundation of China (81860497 to QT), and the Applied Basic Research Programs of Science and Technology Commission Foundation of Yunnan Province (202201AT070117 to QT).

Availability of data and materials

Mass spectrometry data is available at Proteome Xchange, Project accession: PXD032951. The data sets used and/or analyzed during the current study are available from the corresponding author on reasonable request.

Declarations

Ethics approval and consent to participate

All experiments conducted on animals were approved by the Institutional Animal Care and Use Committee of Kunming Institute of Zoology, Chinese Academy of Sciences. All clinical samples used in this study were approved by the Committee for Ethical Review of Research Involving Human Subjects at the Second Affiliated Hospital of Kunming Medical University.

Consent for publication

Not applicable.

Competing interests

The authors declared no competing interests.

Author details

¹Kunming Institute of Zoology, Chinese Academy of Sciences, Kunming, China. ²Key Laboratory of Animal Models and Human Disease Mechanisms of Yunnan Province, Kunming Institute of Zoology, Chinese Academy of Sciences, Kunming, China. ³University of Chinese Academy of Sciences, Beijing, China. ⁴State Key Laboratory of Genetic Resources and Evolution, Kunming Institute of Zoology, Chinese Academy of Sciences, Kunming, China. ⁵Center for Excellence in Animal Evolution and Genetics, Chinese Academy of Sciences, Kunming, China. ⁶Department of Hepatobiliary and Pancreatic Surgery, Second Affiliated Hospital of Kunming Medical University, Kunming, China. ⁷Jiangsu Key Laboratory of Neuropsychiatric Diseases and College of Pharmaceutical Sciences, Jiangsu Key Laboratory of Preventive and Translational Medicine for Geriatric Diseases, Soochow University, Soochow, China. ⁸Primate Facility, National Research Facility for Phenotypic & Genetic Analysis of Model Animals, and National Resource Center for Non-Human Primates, Kunming Institute of Zoology, Chinese Academy of Sciences, Kunming, China.

Received: 29 June 2022 Accepted: 7 September 2022

Published online: 15 September 2022

References

- Shah VM, Sheppard BC, Sears RC, Alani AW. Hypoxia: friend or foe for drug delivery in pancreatic Cancer. *Cancer Lett.* 2020;492:63–70.
- Muz B, de la Puente P, Azab F, Azab AK. The role of hypoxia in cancer progression, angiogenesis, metastasis, and resistance to therapy. *Hypoxia (Auckl).* 2015;3:83–92.
- Tao J, Yang G, Zhou W, Qiu J, Chen G, Luo W, et al. Targeting hypoxic tumor microenvironment in pancreatic cancer. *J Hematol Oncol.* 2021;14:14.
- Halbrook CJ, Lyssiotis CA. Employing metabolism to improve the diagnosis and treatment of pancreatic Cancer. *Cancer Cell.* 2017;31:5–19.
- Guillaume F, Leca J, Olivares O, Lavaut MN, Vidal N, Berthezene P, et al. Strengthened glycolysis under hypoxia supports tumor symbiosis and hexosamine biosynthesis in pancreatic adenocarcinoma. *Proc Natl Acad Sci U S A.* 2013;110:3919–24.
- Lei J, Huo X, Duan W, Xu Q, Li R, Ma J, et al. Alpha-Mangostin inhibits hypoxia-driven ROS-induced PSC activation and pancreatic cancer cell invasion. *Cancer Lett.* 2014;347:129–38.
- Zhu H, Wang D, Liu Y, Su Z, Zhang L, Chen F, et al. Role of the hypoxia-inducible factor-1 alpha induced autophagy in the conversion of non-stem pancreatic cancer cells into CD133+ pancreatic cancer stem-like cells. *Cancer Cell Int.* 2013;13:119.
- Su Y, Loos M, Giese N, Hines OJ, Diebold I, Gorchal A, et al. PHD3 regulates differentiation, tumour growth and angiogenesis in pancreatic cancer. *Br J Cancer.* 2010;103:1571–9.
- Yamasaki A, Yanai K, Onishi H. Hypoxia and pancreatic ductal adenocarcinoma. *Cancer Lett.* 2020;484:9–15.
- Kishimoto S, Brender JR, Chandramouli GVR, Saida Y, Yamamoto K, Mitchell JB, et al. Hypoxia-activated Prodrug Evofosfamide treatment in pancreatic ductal adenocarcinoma Xenografts alters the tumor redox status to potentiate radiotherapy. *Antioxid Redox Signal.* 2021;35:904–15.
- Koc A, Wheeler LJ, Mathews CK, Merrill GF. Hydroxyurea arrests DNA replication by a mechanism that preserves basal dNTP pools. *J Biol Chem.* 2004;279:223–30.
- Smith SC, Petrova AV, Madden MZ, Wang HY, Pan YF, Warren MD, et al. A gemcitabine sensitivity screen identifies a role for NEK9 in the replication stress response. *Nucleic Acids Res.* 2014;42:11517–27.
- Conroy T, Desseigne F, Ychou M, Bouche O, Guimbaud R, Becouarn Y, et al. FOLFIRINOX versus gemcitabine for metastatic pancreatic Cancer. *N Engl J Med.* 2011;364:1817–25.
- Oettle H, Post S, Neuhaus P, Gellert K, Langrehr J, Ridwelski K, et al. Adjuvant chemotherapy with gemcitabine vs observation in patients undergoing curative-intent resection of pancreatic cancer - a randomized controlled trial. *JAMA.* 2007;297:267–77.
- Mathews CK. Deoxyribonucleotide metabolism, mutagenesis and cancer. *Nat Rev Cancer.* 2015;15:528–39.
- Ng N, Purshouse K, Foskolou IP, Olcina MM, Hammond EM. Challenges to DNA replication in hypoxic conditions. *FEBS J.* 2018;285:1563–71.
- Foskolou IP, Jorgensen C, Leszczynska KB, Olcina MM, Tarhonskaya H, Haisma B, et al. Ribonucleotide Reductase requires subunit switching in hypoxia to maintain DNA replication. *Mol Cell.* 2017;66:206–20 e9.
- Huang P, Chubb S, Hertel LW, Grindley GB, Plunkett W. Action of 2',2'-Difluorodeoxycytidine on DNA-synthesis. *Cancer Res.* 1991;51:6110–7.
- Lans H, Hoeijmakers JHJ, Vermeulen W, Marteijn JA. The DNA damage response to transcription stress. *Nat Rev Mol Cell Biol.* 2019;20:766–84.
- Petermann E, Lan L, Zou L. Sources, resolution and physiological relevance of R-loops and RNA-DNA hybrids. *Nat Rev Mol Cell Biol.* 2022;23:521–40.
- Drolet M, Brochu J. R-loop-dependent replication and genomic instability in bacteria. *DNA Repair.* 2019;84:102693.
- Perez-Calero C, Bayona-Feliu A, Xue XY, Barroso SI, Munoz S, Gonzalez-Basallote VM, et al. UAP56/DDX39B is a major cotranscriptional RNA-DNA helicase that unwinds harmful R loops genome-wide (vol 34, pg 898, 2020). *Genes Dev.* 2021;35:573.
- McIntosh D, Blow JJ. Dormant origins, the licensing checkpoint, and the response to replicative stresses. *Cold Spring Harb Perspect Biol.* 2012;4:a012955.
- Lopes M, Foiani M, Sogo JM. Multiple mechanisms control chromosome integrity after replication fork uncoupling and restart at irreparable UV lesions. *Mol Cell.* 2006;21:15–27.
- Zeman MK, Cimprich KA. Causes and consequences of replication stress. *Nat Cell Biol.* 2014;16:2–9.
- Moise AR, Kuksa V, Imanishi Y, Palczewski K. Identification of all-trans-retinol: all-trans-13,14-dihydroretinol saturase. *J Biol Chem.* 2004;279:50230–42.
- Sun Y, Ng L, Lam W, Lo CKC, Chan PT, Yuen YL, et al. Identification and characterization of a novel mouse peroxisome proliferator-activated receptor alpha-regulated and starvation-induced gene, Ppsig. *Int J Biochem Cell Biol.* 2008;40:1775–91.
- Schupp M, Lefterova MI, Janke J, Leitner K, Cristancho AG, Mullican SE, et al. Retinol saturase promotes adipogenesis and is downregulated in obesity. *Proc Natl Acad Sci U S A.* 2009;106:1105–10.
- Shin DJ, Joshi P, Hong SH, Mosure K, Shin DG, Osborne TF. Genome-wide analysis of FoxO1 binding in hepatic chromatin: potential involvement of FoxO1 in linking retinoid signaling to hepatic gluconeogenesis. *Nucleic Acids Res.* 2012;40:11499–509.
- Weber P, Flores RE, Kiefer MF, Schupp M. Retinol Saturase: more than the name suggests. *Trends Pharmacol Sci.* 2020;41:418–27.
- Nagaoka-Yasuda R, Matsuo N, Perkins B, Limbaeck-Stokin K, Mayford M. An RNAi-based genetic screen for oxidative stress resistance reveals retinol saturase as a mediator of stress resistance. *Free Radic Biol Med.* 2007;43:781–8.
- Xu D, Yang C, Shen Q, Pan S, Liu Z, Zhang T, et al. A single mutation underlying phenotypic convergence for hypoxia adaptation on the Qinghai-Tibetan plateau. *Cell Res.* 2021;31:1032–5.
- Chan JYK, Poon PHY, Zhang Y, Ng CWK, Piao WY, Ma M, et al. Case report: exome sequencing reveals recurrent RETSAT mutations and a loss-of-function POLDIP2 mutation in a rare undifferentiated tongue sarcoma. *F1000Res.* 2018;7:499.
- Jiang XL, He YM, Shen QS, Duan LC, Yuan YX, Tang L, et al. RETSAT mutation selected for hypoxia adaptation inhibits tumor growth. *Front Cell Dev Biol.* 2021;9:744992.
- Heidenreich S, Witte N, Weber P, Goehring I, Tolkachov A, von Loeffelholz C, et al. Retinol saturase coordinates liver metabolism by regulating ChREBP activity. *Nat Commun.* 2017;8:384.
- Zhao B, Zhang WD, Duan YL, Lu YQ, Cun YX, Li CH, et al. Filia is an ESC-specific regulator of DNA damage response and safeguards genomic stability. *Cell Stem Cell.* 2015;16:684–98.
- Tu Q, Hao J, Zhou X, Yan L, Dai H, Sun B, et al. CDKN2B deletion is essential for pancreatic cancer development instead of unmeaningful co-deletion due to juxtaposition to CDKN2A. *Oncogene.* 2018;37:128–38.

38. Yang D, Sun B, Zhang XH, Cheng DM, Yu XP, Yan LZ, et al. Huwe1 sustains Normal ovarian epithelial cell transformation and tumor growth through the histone H1.3-H19 Cascade. *Cancer Res*. 2017;77:4773–84.
39. Swain U, Rao KS. Study of DNA damage via the comet assay and base excision repair activities in rat brain neurons and astrocytes during aging. *Mech Ageing Dev*. 2011;132:374–81.
40. Zhao B, Zhang WD, Cun YX, Li JZ, Liu Y, Gao J, et al. Mouse embryonic stem cells have increased capacity for replication fork restart driven by the specific Fila-Floped protein complex. *Cell Res*. 2018;28:69–89.
41. Sirbu BM, Couch FB, Cortez D. Monitoring the spatiotemporal dynamics of proteins at replication forks and in assembled chromatin using isolation of proteins on nascent DNA. *Nat Protoc*. 2012;7:594–605.
42. Sirbu BM, Couch FB, Feigerle JT, Bhaskara S, Hiebert SW, Cortez D. Analysis of protein dynamics at active, stalled, and collapsed replication forks. *Genes Dev*. 2011;25:1320–7.
43. Shevchenko A, Wilm M, Vorm O, Mann M. Mass spectrometric sequencing of proteins from silver stained polyacrylamide gels. *Anal Chem*. 1996;68:850–8.
44. Zhu Y, Lei Q, Li D, Zhang Y, Jiang X, Hu Z, et al. Proteomic and biochemical analyses reveal a novel mechanism for promoting protein Ubiquitination and degradation by UFBP1, a key component of Ufmlylation. *J Proteome Res*. 2018;17:1509–20.
45. Zeeberg K, Cardone RA, Greco MR, Saccomano M, Nohr-Nielsen A, Alves F, et al. Assessment of different 3D culture systems to study tumor phenotype and chemosensitivity in pancreatic ductal adenocarcinoma. *Int J Oncol*. 2016;49:243–52.
46. Boj SF, Hwang CI, Baker LA, Chio IIC, Engle DD, Corbo V, et al. Organoid models of human and mouse ductal pancreatic Cancer. *Cell*. 2015;160:324–38.
47. Huang L, Holtzinger A, Jagan I, BeGora M, Lohse I, Ngai N, et al. Ductal pancreatic cancer modeling and drug screening using human pluripotent stem cell- and patient-derived tumor organoids. *Nat Med*. 2015;21:1364–71.
48. Koikawa K, Ohuchida K, Ando Y, Kibe S, Nakayama H, Takesue S, et al. Basement membrane destruction by pancreatic stellate cells leads to local invasion in pancreatic ductal adenocarcinoma. *Cancer Lett*. 2018;425:65–77.
49. Sun C, Yamato T, Furukawa T, Ohnishi Y, Kijima H, Horii A. Characterization of the mutations of the K-ras, p53, p16, and SMAD4 genes in 15 human pancreatic cancer cell lines. *Oncol Rep*. 2001;8:89–92.
50. Koong AC, Mehta VK, Le QT, Fisher GA, Terris DJ, Brown JM, et al. Pancreatic tumors show high levels of hypoxia. *Int J Radiat Oncol Biol Phys*. 2000;48:919–22.
51. Welsh S, Williams R, Kirkpatrick L, Paine-Murrieta G, Powis G. Antitumor activity and pharmacodynamic properties of PX-478, an inhibitor of hypoxia-inducible factor-1alpha. *Mol Cancer Ther*. 2004;3:233–44.
52. McDonald PC, Chafe SC, Brown WS, Saberi S, Swayampakula M, Venkateswaran G, et al. Regulation of pH by carbonic anhydrase 9 mediates survival of pancreatic Cancer cells with activated KRAS in response to hypoxia. *Gastroenterology*. 2019;157:823–37.
53. Zhao B, Lin JH, Rong LJ, Wu S, Deng Z, Fatkhutdinov N, et al. ARID1A promotes genomic stability through protecting telomere cohesion. *Nat Commun*. 2019;10:4067.
54. Schlacher K, Christ N, Siaud N, Egashira A, Wu H, Jasin M. Double-Strand break repair-independent role for BRCA2 in blocking stalled replication fork degradation by MRE11. *Cell*. 2011;145:529–42.
55. Halliwell JA, Gravells P, Bryant HE. DNA Fiber assay for the analysis of DNA replication progression in human pluripotent stem cells. *Curr Protoc Stem Cell Biol*. 2020;54:e115.
56. Davies SL, North PS, Hickson ID. Role for BLM in replication-fork restart and suppression of origin firing after replicative stress. *Nat Struct Mol Biol*. 2007;14:677–9.
57. Ciccia A, Bredemeyer AL, Sowa ME, Terret ME, Jallepalli PV, Harper JW, et al. The SPOD disorder protein SMARCAL1 is an RPA-interacting protein involved in replication fork restart. *Genes Dev*. 2009;23:2415–25.
58. Briu LM, Maric C, Cadoret JC. Replication stress, genomic instability, and replication timing: a complex relationship. *Int J Mol Sci*. 2021;22:4764.
59. Lukasova E, Rezacova M, Bacikova A, Sebejova L, Vavrova J, Kozubek S. Distinct cellular responses to replication stress leading to apoptosis or senescence. *FEBS Open Bio*. 2019;9:870–90.
60. Blasina A, Hallin J, Chen E, Arango ME, Kraynov E, Register J, et al. Breaching the DNA damage checkpoint via PF-0047736, a novel small-molecule inhibitor of checkpoint kinase 1. *Mol Cancer Ther*. 2008;7:2394–404.
61. Zhang HN, He CC, Guo XX, Fang YX, Lai QH, Wang XK, et al. DDX39B contributes to the proliferation of colorectal cancer through direct binding to CDK6/CCND1. *Cell Death Dis*. 2022;8:30.
62. Yoo HH, Chung IK. Requirement of DDX39 DEAD box RNA helicase for genome integrity and telomere protection. *Aging Cell*. 2011;10:557–71.
63. Dymock BW, Barril X, Brough PA, Cansfield JE, Massey A, McDonald E, et al. Novel, potent small-molecule inhibitors of the molecular chaperone Hsp90 discovered through structure-based design. *J Med Chem*. 2005;48:4212–5.
64. Schumann S, Jackson BR, Yule I, Whitehead SK, Revill C, Foster R, et al. Targeting the ATP-dependent formation of herpesvirus ribonucleoprotein particle assembly as an antiviral approach. *Nature. Microbiology*. 2017;2:16201.
65. Ewers KM, Patil S, Kopp W, Thomale J, Quilitz T, Magerhans A, et al. HSP90 inhibition synergizes with Cisplatin to eliminate basal-like pancreatic ductal adenocarcinoma cells. *Cancers (Basel)*. 2021;13:6163.
66. Zhang Y, Ware MB, Zaidi MY, Ruggieri AN, Olson BM, Komar H, et al. Heat shock Protein-90 inhibition alters activation of pancreatic stellate cells and enhances the efficacy of PD-1 blockade in pancreatic Cancer. *Mol Cancer Ther*. 2021;20:150–60.

Publisher's Note

Springer Nature remains neutral with regard to jurisdictional claims in published maps and institutional affiliations.

Ready to submit your research? Choose BMC and benefit from:

- fast, convenient online submission
- thorough peer review by experienced researchers in your field
- rapid publication on acceptance
- support for research data, including large and complex data types
- gold Open Access which fosters wider collaboration and increased citations
- maximum visibility for your research: over 100M website views per year

At BMC, research is always in progress.

Learn more biomedcentral.com/submissions

